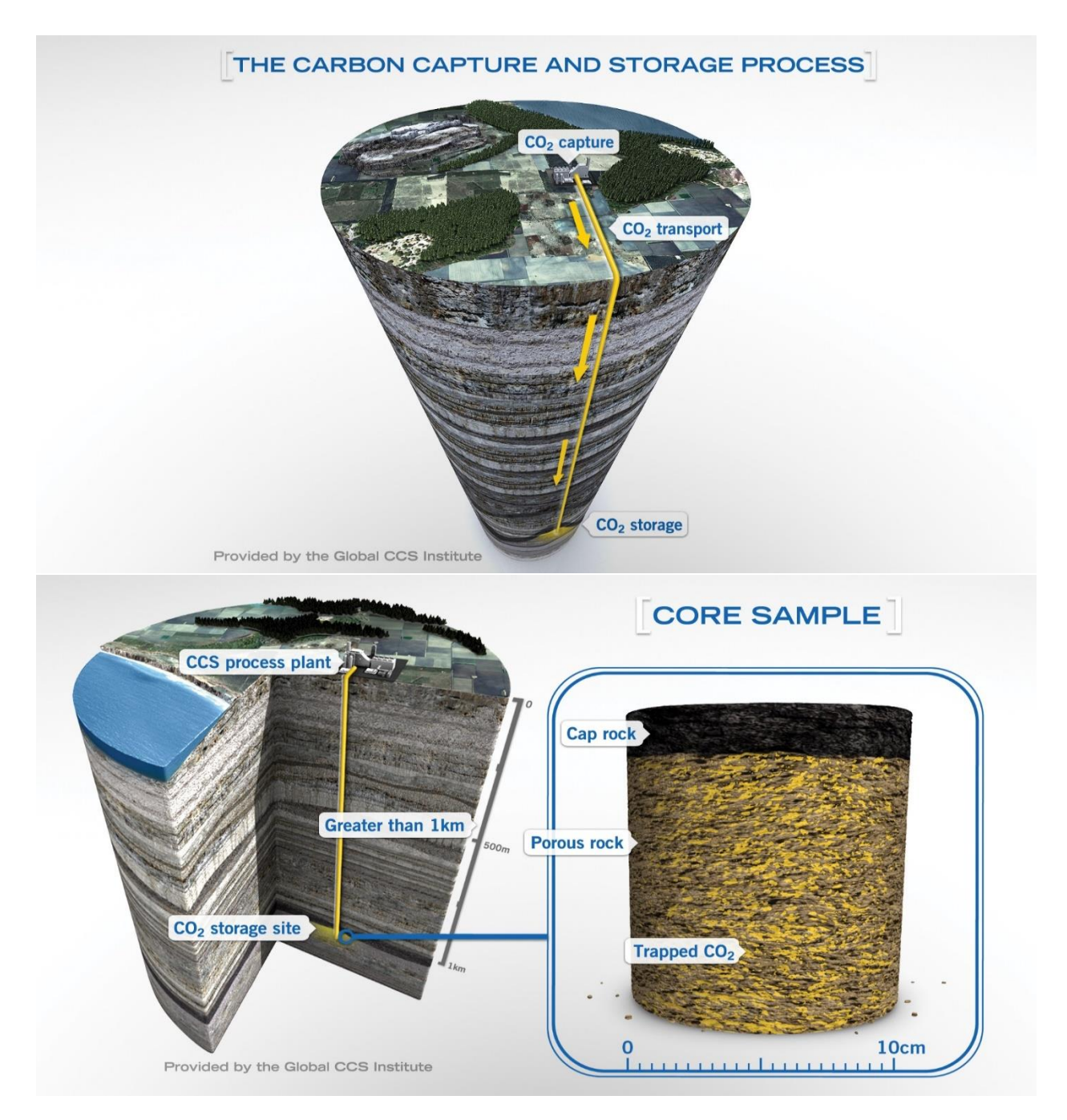
Lower Buntsandstein Subgroup sealing potential in the southern Dutch offshore



Internship project by Alexandros Freiderikos

Supervisors: Dr. Aart-Peter van der Berg van Saparoea and Daan den Hartog Jager (EBN B.V)

Profs. Liviu Matenco and Fred Beekman (UU)

Contents

Abstract	3
Introduction	4
Geological Background	5
Stratigraphy	5
Depositional history	8
Tectonic evolution	10
Methodology	12
Structural analysis	15
Well correlation	15
Thickness maps	19
Depth maps	21
Compositional analysis	22
RBSM Lithology	22
Porosity/Permeability plots	25
Sealing capacity evaluation	27
Structural maps of known fields	27
Sealing capacity measurements (MITs)	29
Overpressure analysis	30
Discussion	32
Gross Depositional Environment (GDE) map of the RBSM	32
Sealing capacity map and sealing potential of RBSM	34
Recommendations for further study	35
Conclusions	36
Acknowledgements	36
References	37
Annandiy	20

Abstract

This study evaluates the sealing potential of the Main Claystone Formation (RBSM) of the Lower Buntsandstein Subgroup in the southern Dutch offshore, a key consideration for CO₂ storage in depleted Permian reservoirs lacking the conventional top seal, the Zechstein evaporites. Detailed stratigraphic, structural and compositional analyses were performed on over 160 NL and UK, both offshore and onshore, wells using Petrel and QGIS, integrating thickness and depth mapping, lithological interpretation and overpressure analysis. Regional sealing capacity evaluation followed, incorporating legacy structural data of depleted fields to infer the maximum column heights of CO2 that can be maintained as well as direct core sealing capacity measurements in the laboratory using Mercury Injection Tests (MIT). The RBSM comprises deeply buried, illite- and anhydrite-rich claystones with minimal porosity and permeability, whose sealing capacity is primarily governed by lithology, anhydrite content, compaction and stratification. Structural controls, notably early Cretaceous uplift and erosion associated with the Winterton High's presence, locally compromise seal integrity, while central and eastern areas dominated by massive-blocky or laminated claystone-shale facies support CO₂ columns of 360-465 m, exceeding 465 m toward the north and northeast. Sealing effectiveness diminishes to ≤145 m in regions with sandier facies or severe erosion (Winterton High). Overpressure indicators identified within the formation also reinforce the robust sealing behavior regionally. The findings redefine the Main Claystone as a reliable regional top seal and support its inclusion in risk assessments for CO₂ storage, with implications for expanding storage capacity in the southern Dutch offshore.

Introduction

A good understanding of the presence and quality of sealing lithologies is highly relevant for accessing CO₂ storage potential in depleted fields or aquifers of the Dutch offshore. The Rotliegend and Zechstein (Permian) are very important reservoir units in The Netherlands. Typically for these reservoirs, the Zechstein evaporites (upper Permian) are the most common and proven top seal. In the south of the Netherlands, however, these evaporites are not present (hatched yellow area in Figure 1). The next stratigraphic unit that could constitute an effective seal is the Main Claystone Formation (Induan, early Triassic). The uppermost Zechstein unit-the Zechstein Upper Claystone formation, could also contribute in sealing on top although it is usually extremely thin to effectively seal independently. Nevertheless, the former unit was deposited in a continental basin. Often this type of deposit has insufficient sealing capacity

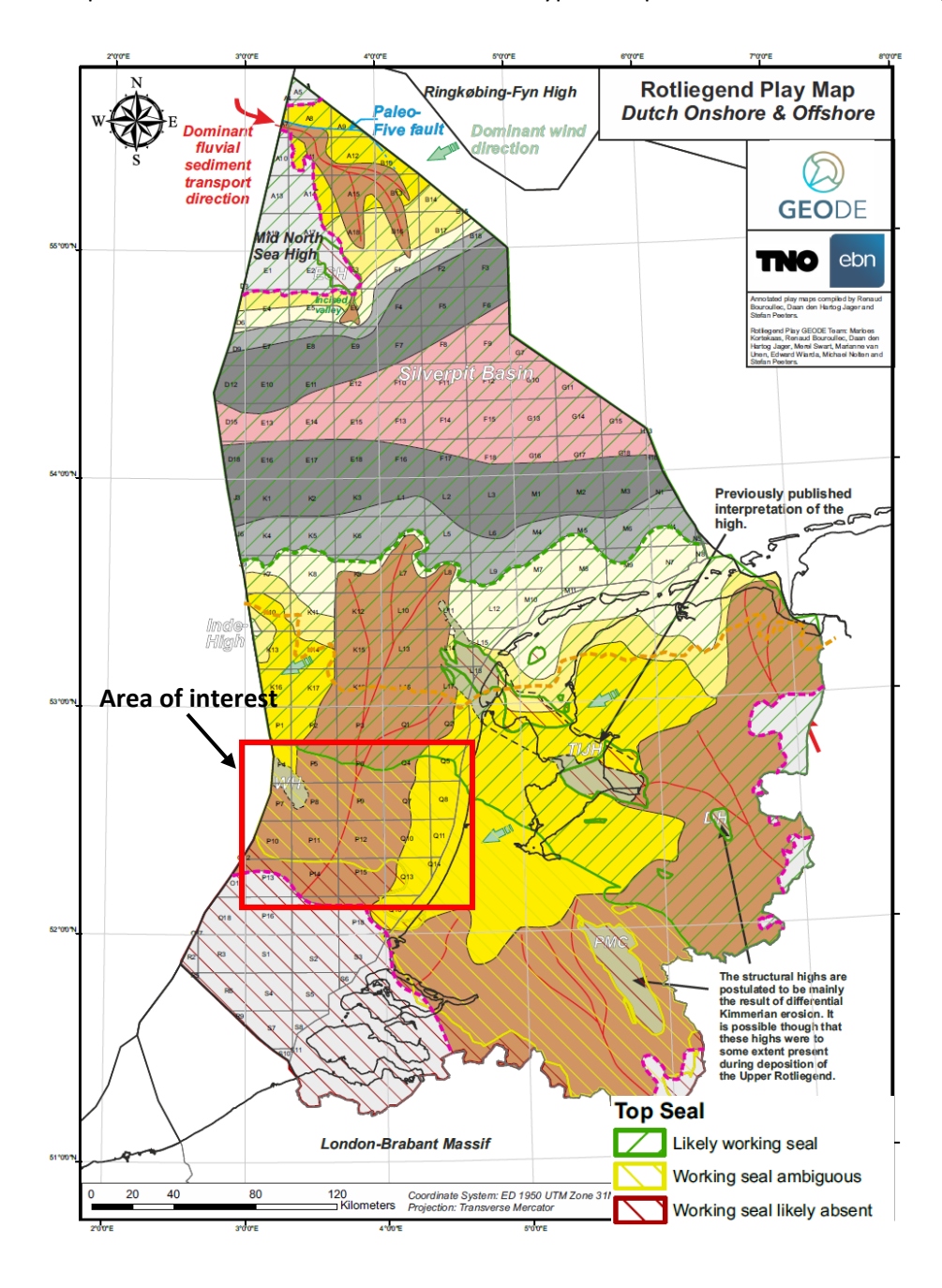


Figure 1: GDE map of the Rotliegend in the Netherlands. The hatched polygons indicate areas where the top seal is very likely to work (in green; this area matches the presence of Zechstein evaporites), areas where effective top seal is ambiguous (in yellow), and areas where top seal is probably absent (in red, Kortekaas et al., 2023, GEODE Atlas).

to trap significant volumes of CO₂. The Rotliegend and Zechstein reservoirs in this area were therefore long assumed to have no effective top seal.

The successful developments of the P11b De Ruyter (2006) and Q10-A fields (2019, Fig. 1) demonstrated that the Main Claystone Formation can in fact be an effective top seal. Evaluating the sealing potential of the Main Claystone Formation is therefore highly relevant to the activities of EBN. The study area (red circle in Figure 1) is potentially interesting for the storage of CO₂ in aquifers or depleted fields because of its location, offshore and close to the Rotterdam harbor.

On this basis, the main research question is whether the Q10-A field is the result of a unique combination of local factors, or if the Main Claystone Formation has sealing potential over the entire area of interest. In such a case, what the minimal CO₂ column is that this seal can hold and does the sealing capacity of the Main Claystone Formation vary across the area of interest? Finally, if the sealing capacity of the Main Claystone Formation varies, can this variability be predicted? Within this framework, the list of deliverables for the current study are:

- 1) A summary of gas-water contacts and sealing units in the Q10-A and P06-Main fields (and other minor fields),
- 2) A summary of sealing capacity tests in the area of interest,
- 3) A summary of available data on the composition and sealing capacity of the Main Claystone Formation in the area of interest,
- 4) An analysis of the sealing capacity of the Main Claystone Formation in the area of interest,
- 5) Recommendations on exploration and/or further study.

Geological Background

Stratigraphy

The Triassic stratigraphy in the Netherlands is defined by the Germanic Trias Group, characterized by the classical tripartite division into Bunter, Muschelkalk and Keuper units (Fig. 2A). While an upward clastic-carbonate-clastic lithologies respectively is accepted, the specific facies development and timing exhibit regional variations (McKie and Kilhams 2025). Three prominent, regional, unconformities occur: the Hardegsen, the Early Cimmerian I and II unconformities (Fig. 2A, Geluk 2005). Since 1980, the typical subdivision of the Triassic sequence in the Netherlands is between two groups:

• The Lower Germanic Trias Group (Fig. 2A), comprises the Lower and Main Buntsandstein subgroups. The Lower Buntsandstein consists primarily of the Main Claystone Formation, representing a dry lake claystone facies, overlain by the Rogenstein Formation, characterized by similar playa claystone with interbedded oolitic facies. The lithostratigraphic base of this group is

typically picked at the sand prone top of the Zechstein Upper Claystone. Nevertheless, the actual Permian—Triassic boundary may occur stratigraphically higher (or lower). The Main Buntsandstein Subgroup includes interbedded sandstones and shales of the Volpriehausen, Detfurth and Hardegsen formations. The top of the group is marked by the Base Solling (Hardegsen) Unconformity (Fig. 2B).

• The Upper Germanic Trias Group (Fig. 2A) comprises an alternation of fine-grained clastic deposits and evaporites within the Solling and Rot formations, followed by carbonate and evaporite facies representing the Muschelkalk Formation. The upward succession continues with a predominantly fine-grained interval locally containing anhydrite and halite, with subordinate sandstone layers, of the Keuper Formation (Fig. 2B, McKie and Kilhams 2025)

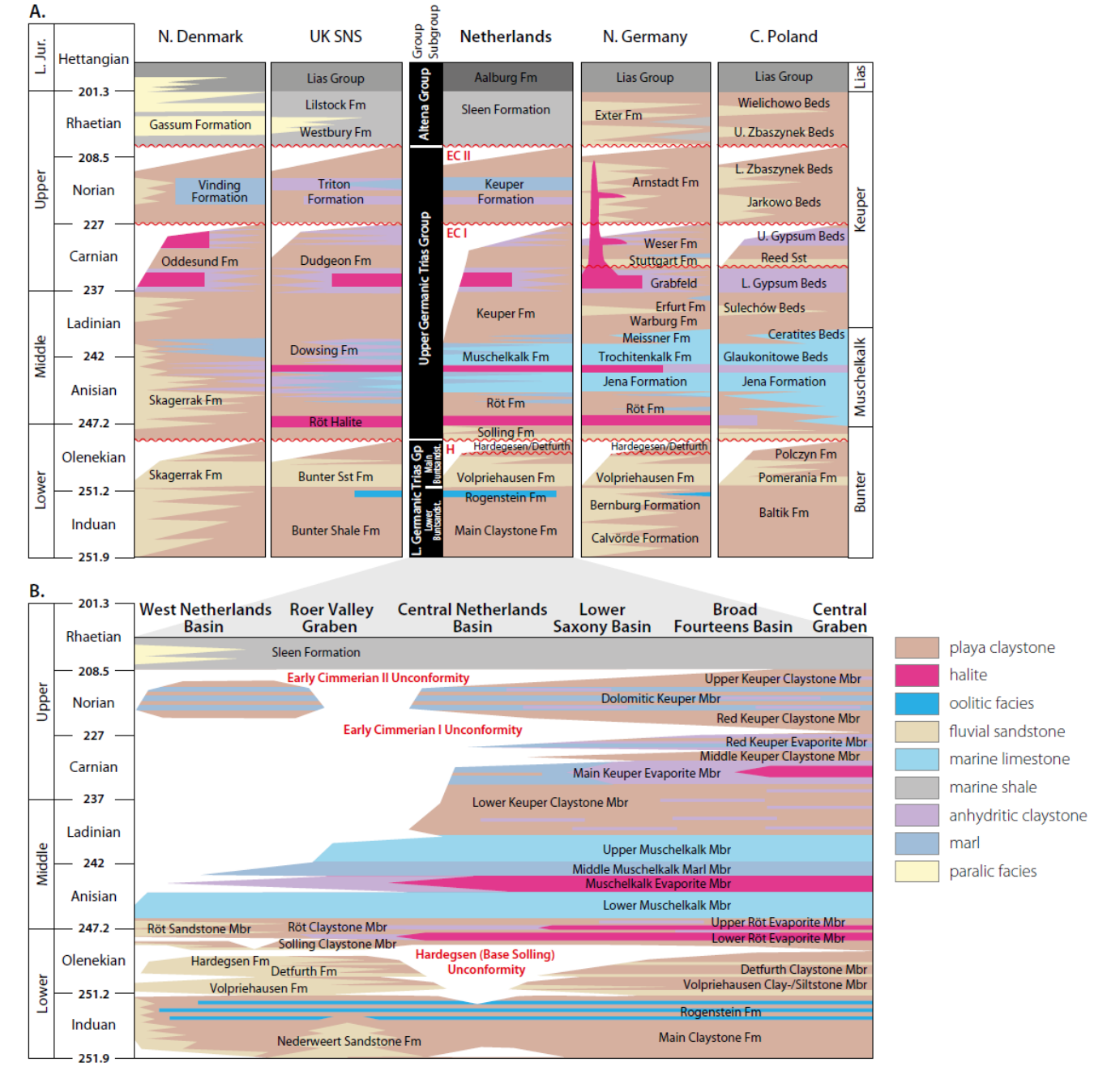


Figure 2: The stratigraphy and dominant facies of the Triassic succession. a) Overview of the stratigraphy in the Netherlands and comparison with adjacent areas. b) Detailed stratigraphy of the Triassic in the Netherlands (McKie and Kilhams 2025, Geology of the Netherlands book).

The lower predominantly clastic unit of the Germanic Triassic succession, represented by the Buntsandstein, was deposited from the Late Permian to Early Anisian within a broad intra-cratonic basin under fluvio-lacustrine conditions, with minor marine influence limited to its uppermost intervals (Aigner & Bachmann 1992, Van Adrichem Boogaert & Kouwe 1994). The total thickness of the Buntsandstein succession generally averages 300m in NL with a maximum value of 900m (Kortekaas et al., 2023, GEODE Atlas). Originally, during deposition, its thickness is expected to have been between 500m and 1000m but later reduced by the Cimmerian erosion (Geluk & Röhling, 1997). The succession is largely non-fossiliferous and is characterized by widespread soft-sediment deformation, mud cracks and evidence of secondary reddening or reduction. Oolitic limestones within the Lower and Middle Buntsandstein are interpreted to have formed in a slightly saline water setting (Peryt 1975, Palermo et al. 2008). Cyclic patterns observed in the continental basin successions are likely not linked to eustatic sea-level fluctuations, but rather to climatic variations associated with Milankovitch cycles (Geluk & Röhling, 1997).

The Lower Buntsandstein Formation is an easily identifiable unit on wireline and lithological logs, characterized by a relatively homogeneous succession of siltstones and claystones, typically 300 to 350 meters thick and containing approximately 20 to 25 well-developed fining-upward cycles (Geluk & Röhling, 1997). In its upper part, regionally correlatable oolite beds—composed of either limestone or sandstone—are present. A distinct boundary at the top of the formation, marked by the basal sandstone of the Volpriehausen Formation, represents a minor unconformity. This boundary serves as an important basin-wide marker for correlating Buntsandstein successions (Fig. 3). The formation is dated to the latest Permian—Induan and consists predominantly of mud-rich deposits formed by stacked, upward-cleaning successions. These comprise fine-grained continental siltstones to claystones (Main Claystone), overlain by claystones interspersed with common oolite beds known as the Rogenstein (Palermo et. al., 2008). Individual fining-upward cycles range from 20 to 40 meters in thickness and are laterally continuous across several hundred kilometres (Fig. 3). The Volpriehausen Unconformity, marking the base of the overlying Volpriehausen Formation, locally incises into the Lower Buntsandstein Subgroup by several tens of meters.

Although precise age control is limited due to the continental nature of these deposits, stratigraphic correlation is facilitated by the relatively uniform, layer-cake geometry of the succession across the Netherlands. Furthermore, the presence of distinctive intervals, such as the oolite facies of the Rogenstein, enables reliable regional correlation (Fig. 3, Geluk & Röhling, 1999, Geluk, 2007).

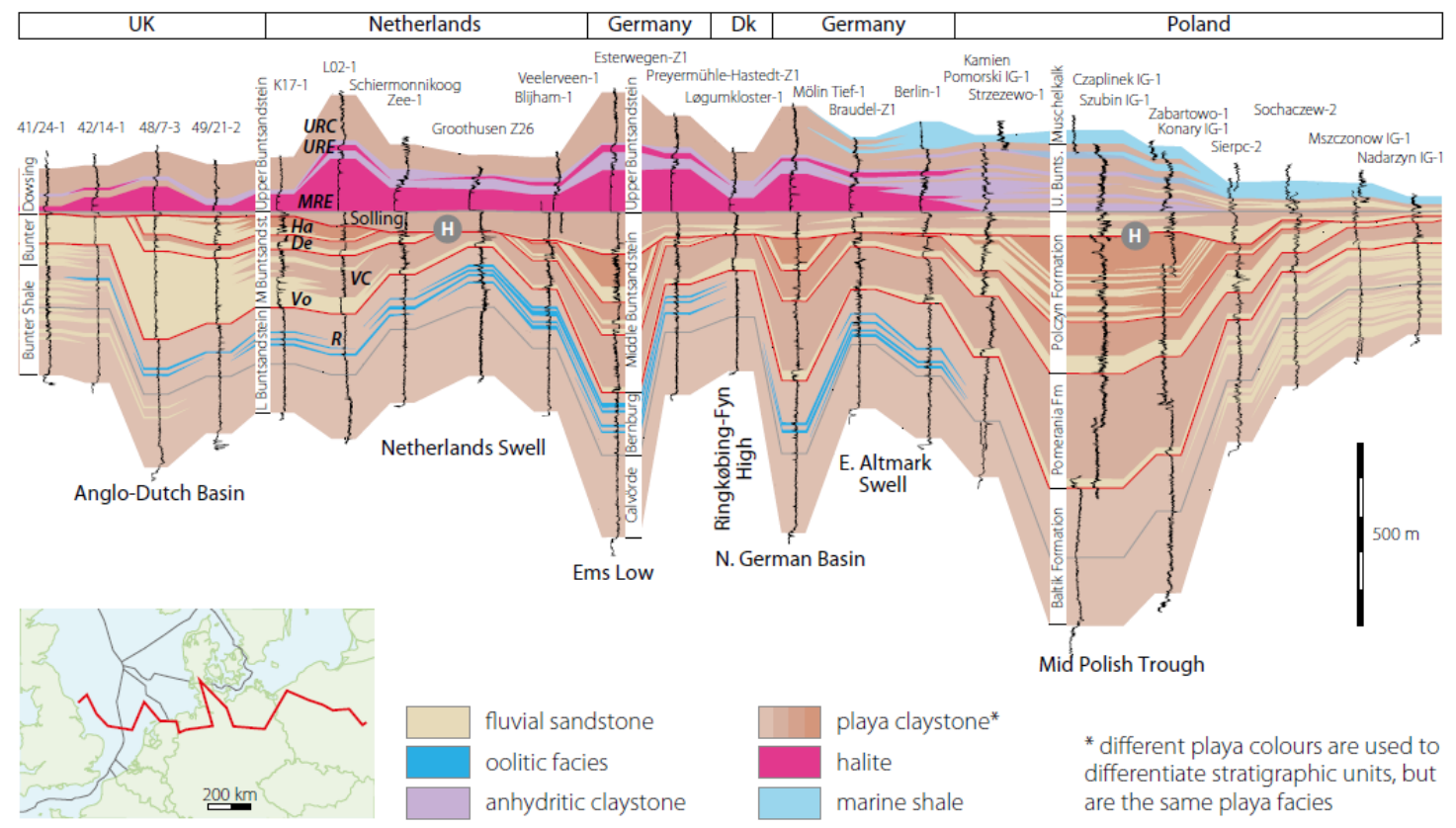


Figure 3: Stratigraphic correlation (based on gamma-ray logs) of the Germanic Trias Group between most of northwestern Europe, flattened on the Early Cimmerian Unconformity I (McKie and Kilhams 2025, Geology of the Netherlands book).

Depositional history

During the Early Triassic, continental clastic sedimentation prevailed across much of northwest Europe, placing the Netherlands within an extensive continental interior, largely isolated from significant marine influence (Fig. 4). The lowermost Triassic unit, the Main Claystone, has been interpreted as representing deposition in ephemeral playa lakes. These lakes were episodically inundated by monsoonal floods, followed by progressive salinization and evaporation. A modern analogue known for the extensive, basin-scale playa systems represented by these facies is the Lake Eyre Basin, Australia (McKie and Kilhams 2025). The Main Claystone is composed of mixed deposits featuring wave and current ripple lamination, massive claystones and occasional coarse-grained sand stringers. Thick sand-prone intervals, such as those of the Nederweert Sandstone Formation, are confined to narrow zones along the southern basin margins in the Netherlands, with isolated sand ribbons extending basin ward from adjacent uplands-London Brabant Massif. During this time, the Roer Valley Graben (RVG) served as the principal axis of fluvial sediment input, while other areas remained largely sand-starved (Fig. 4). The northern onshore and Dutch offshore regions lay predominantly within the central part of the playa system.

Distinct onlitic horizons, up to 5 m thick, are present on top of the Main Claystone and have been collectively defined as the Rogenstein Member. These deposits range from pure onlitic limestones to onlite-bearing sandstones and typically form laterally extensive sheets, with individual beds traceable over

tens of kilometers. They are generally interpreted as shallow-water, lake-margin bar accumulations formed during intervals of sustained high lake levels (max. transgression). However, an alternative interpretation suggests a possible marine influence. The development of oolitic facies marks a notable shift in the basin's hydrological regime toward prolonged subaqueous conditions, interrupted by episodes of playa desiccation. A marine origin, however, would imply basin-wide flooding events, though the source direction remains uncertain.

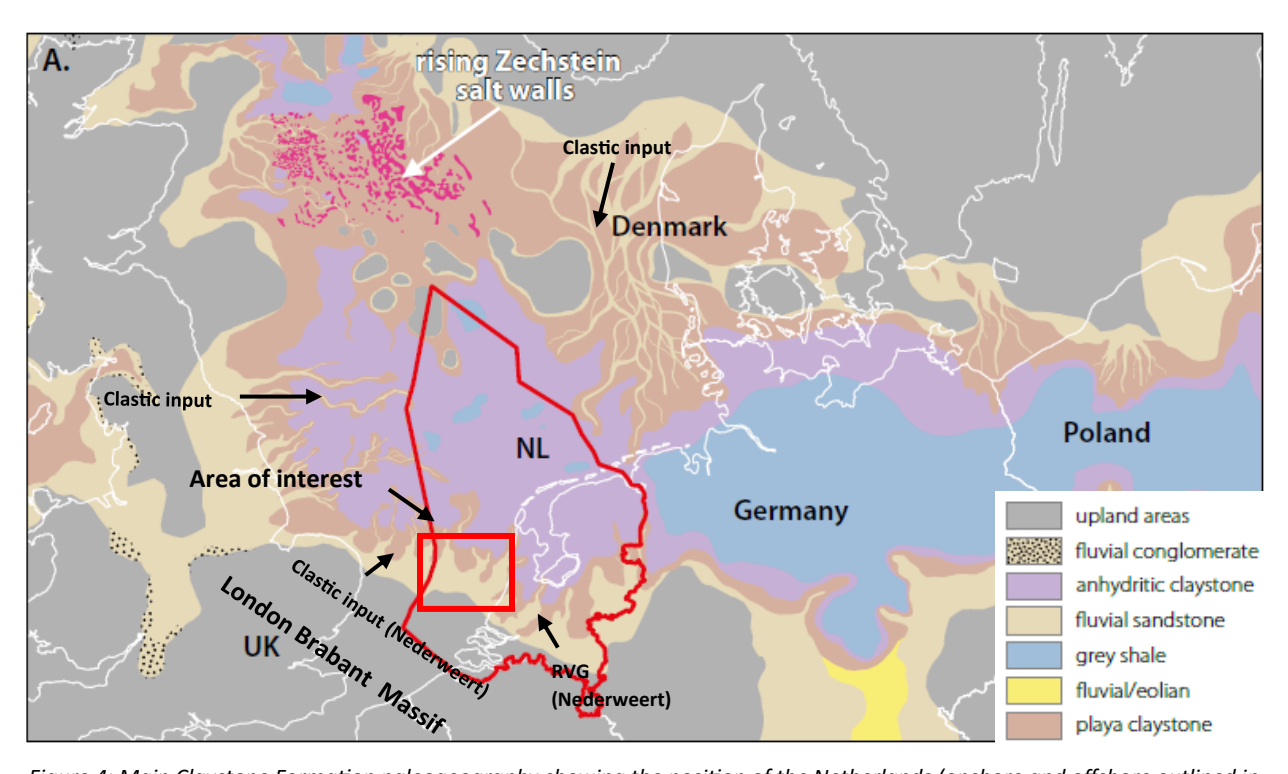
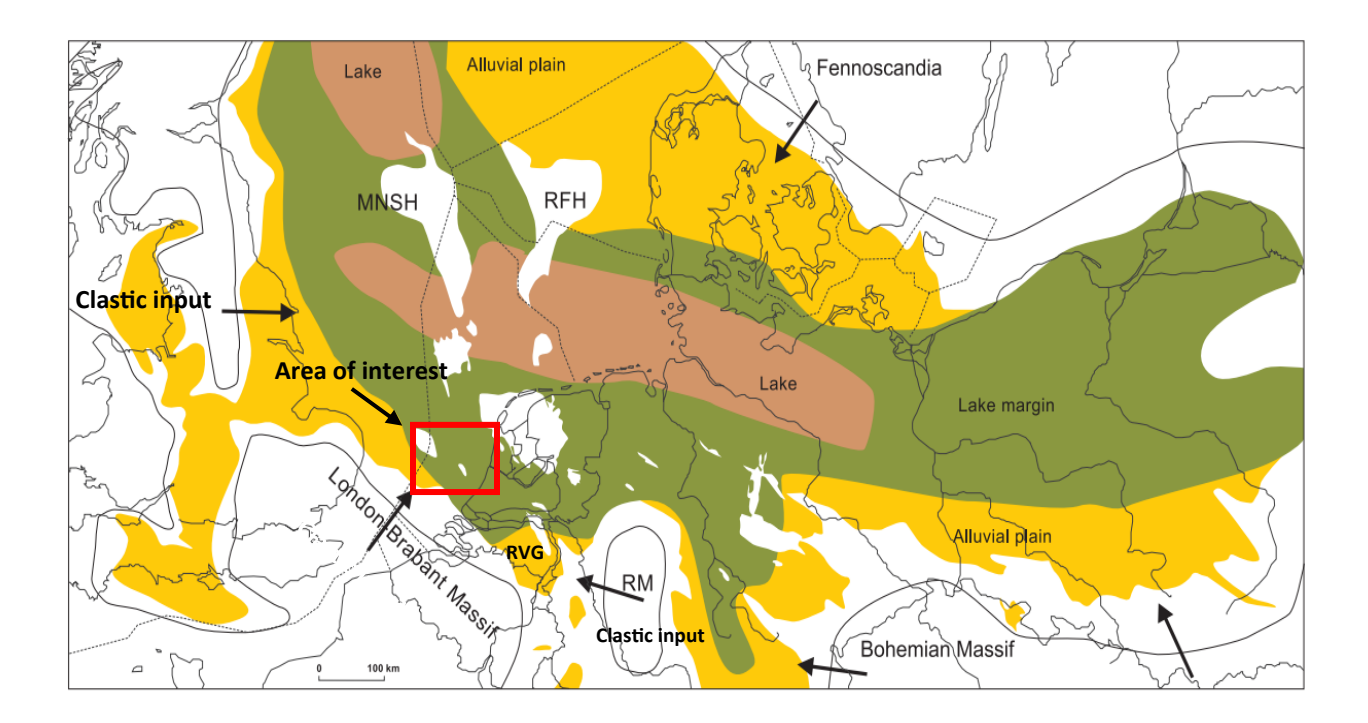


Figure 4: Main Claystone Formation paleogeography showing the position of the Netherlands (onshore and offshore outlined in red) within a vast, muddy playa system (McKie and Kilhams 2025, Geology of the Netherlands book).



Interestingly, the initial facies distribution regional map by Geluk 2005 (Fig. 5), does not include the isolated sand-prone channels extending basin ward. Furthermore, it predicts predominant marginal lake facies (silty-playa claystones) inside the area of interest with only minor alluvial plain, sand-prone facies restricted to the southwestern margin (and the RVG). This contradicts with the more recent facies map proposed by McKie and Kilhams (2025), where a sand dominated Main Claystone covers most of the area of interest with only minor playa claystone facies restricted to the north. However, the source and direction of fluvial clastic input into the paleo-playa lake is consistent between the two regional studies.

Tectonic evolution

The present-day configuration of the Lower Bunter succession was not fully established by the end of the Triassic (Fig. 5). Although no evidence of syn-depositional faulting has been identified (Van Adrichem Boogaert & Kouwe 1994, Geluk & Rohling 1997), the succession underwent significant post-depositional tectonic deformation, subsidence, inversion and dissolution through diagenetic processes. Diagenesis commenced shortly after deposition, marked by sediment compaction, the formation of grain-coating clays and hematite and the precipitation of dolomite from meteoric groundwater percolating through the more permeable, coarser-grained beds. Continued shallow burial (to depths of approximately 500 m) facilitated the migration of more saline fluids, comprising mixtures of meteoric water and brines expelled from deeper claystones and Zechstein evaporites. This process led to the widespread precipitation of anhydrite and halite (Purvis & Okkerman, 1996, McKie and Kilhams 2025).

Continued subsidence throughout the Early Jurassic, accompanied by minor extensional activity localized in the Central Graben and Broad Fourteens Basin (Fig. 6), facilitated ongoing compaction and burial diagenesis. This was marked by the precipitation of quartz, feldspar, ferroan dolomite and authigenic clays: primarily illite and chlorite as burial depth and thermal maturity increased. From the late Middle Jurassic into the Late Jurassic, rifting intensified, with extension focused in the Central and Step Grabens, as well as the West Netherlands, Broad Fourteens, and Terschelling basins (Fig. 6). This phase of accelerated extension drove the Triassic succession to greater burial depths and elevated temperatures. Uplift along rift flanks, particularly of intra-basinal structural highs such as the Winterton High and Winterton Platform within the study area, contributed further to the erosion of Triassic strata.

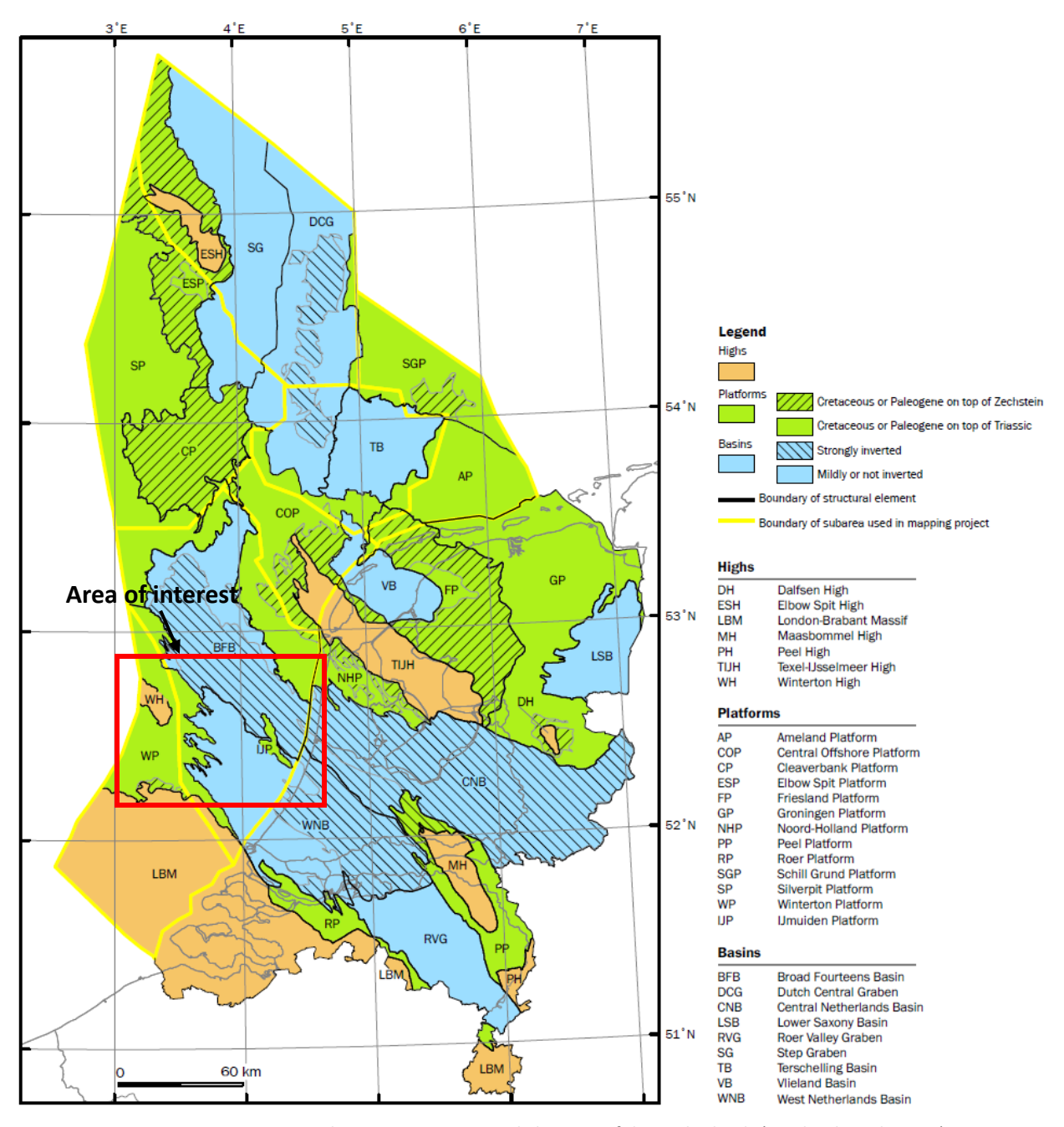


Figure 6: Late Jurassic - Early Cretaceous structural elements of the Netherlands (Kombrink et al., 2012)

During the Late Cretaceous, Alpine compressional events led to the tectonic inversion of the Broad Fourteens, West Netherlands and Central Netherlands basins (Fig. 6). This uplift resulted in localized exposure of the Triassic succession to subaerial erosion and meteoric groundwater infiltration (Kombrink et al., 2012). Interaction with meteoric waters caused dissolution of feldspar and halite along the unconformity surface, accompanied by clay mineral precipitation. The inversion phase also induced significant fracturing within the now-lithified Triassic strata. Subsequent reversion to thermal subsidence

during the early Cenozoic led to renewed burial of the offshore Triassic, whereas the onshore succession remained at relatively shallow depths.

Methodology

Data collection inside the study area initiated, namely, from the national offshore blocks K18-P01-P02-P04 up to Q16 with few onshore wells mostly from the western regions (Alkmaar, Amsterdam, Den Haag) along the coastline (Fig. 7). Public databases, NLOG (NLOG) and DinoLoket (DINOloket) were accessed and stratigraphic-well tops, composite logs, available well measurements or core tests within the Lower Bunter were retrieved. Under this process, over 128 offshore and 35 onshore NL wells were selected with a complete Lower Buntsandstein Formation (Appendix A: Summary of well names, Fig. 7). A similar process was repeated for accessing few internal well log data within EBN. Furthermore, 19 additional publicly available offshore wells from the UK (Appendix A: Summary of well names, Fig. 7), blocks 50-53-54, situated on the south eastern margin close to the Dutch border, were selected and analysed through the North Sea Transition Authority database (NSTA Offshore Activities).

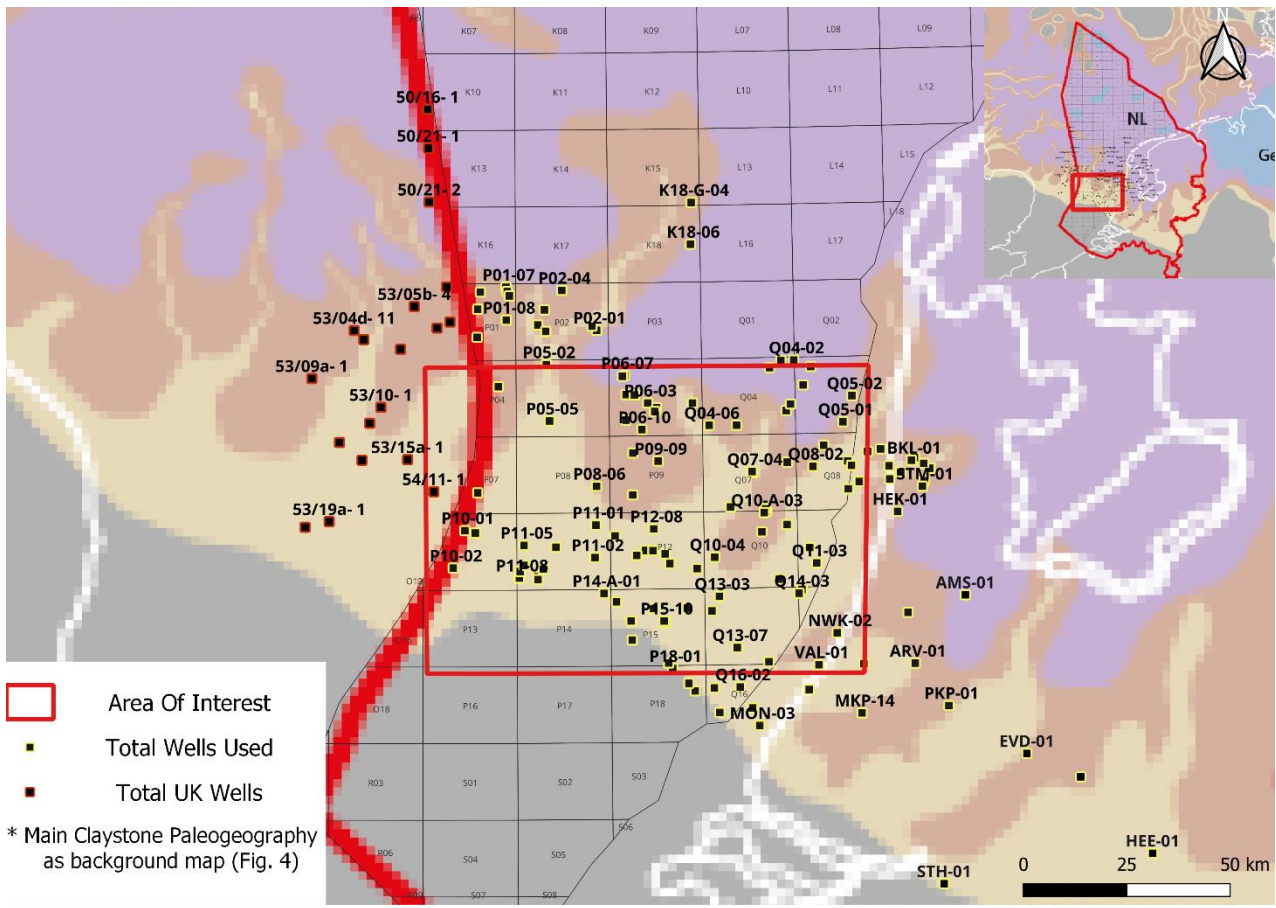


Figure 7: Area of interest (red polygon) with all the wells analysed under the current study. Figure 4 of the proposed paleogeography of the Main Claystone used as a background image in Petrel/QGIS for direct compositional collation.

All the wells selected for the current study were loaded in the Petrel software (Petrel subsurface software | SLB) and later in QGIS (QGIS Web Site) for refined visualization. The area of interest was defined by a rectangle polygon in both projects (Fig. 7, red polygon). Subsequently, well correlation commenced in Petrel with the existing NLOG well tops, combined with the initial composite logs analysis, used as base for the interpretation under this study. Nevertheless, NLOG well tops were regularly inconsistent between distal wells, especially regarding the interpretation of the base and top of the Main Claystone (RBSM) or the Zechstein Upper Claystone (ZEUC) formation thickness. Therefore, adjustments of well tops were made in order to consistently draw the base of ZEUC on top of the anhydrite horizon of the underlying Pegmatite-Anhydrite Zechstein unit, the base of RBSM on the last sandy interface of the underlying ZEUC and the top of RBSM at the base of the first significant oolitic limestone bed of the overlying Rogenstein (RBSR) formation. For the well correlation of the Lower Buntsandstein, gamma-ray and sonic logs were used by preference in well section windows, although in some instances also spontaneous potential and density logs were used successfully. A 1:1000 log-scale supplied enough detail to establish the correlations and identify the base and top of the upper Zechstein Claystone (ZEUC), the Main Claystone (RBSM) and the Rogenstein (RBSR) formations initially, followed by more detailed correlation of specific intervals within the formations. These intervals incorporated dolomitic-limestone horizons, anhydritic bands as well as sand sheets interpreted inside the upper ZE Claystone and the Main Claystone. In the Rogenstein formation, the characteristic, oolitic limestone or sandstone strata were traced (at least four main horizons) and could be correlated across the entire study area.

Based on the interpreted well tops, isochore points were extracted and subsequently thickness maps were developed for the three formations. The 'make surface' option was selected in Petrel using isochore interpolation algorithm bounded by the area of interest polygon as the edge of the model. Thickness maps were also constructed for the four (relatively thin) main oolitic intervals of the Rogenstein formation. Furthermore, depth maps were established for both the RBSM and RBSR following the same process. For all maps, wells with RBSM and RBSR absent were excluded (P04-01, P08-01, P10-04, P11-05, P11-10 and 53_10-01) representing the Winterton High whereas the only selected wells with RBSR or RBSM partially eroded were the P07-01 and P10-01, representing the Winterton Platform. The rest wells around and closer to the Winterton High (P11-03, P11-04 etc.) were not considered for visualisation reasons (they present extremely thin RBSM) and were drawn as part of the edge of the paleo-high.

Next step in the workflow incorporated the lithological analysis mainly of the Main Claystone Formation. This procedure initiated with the lithological data gathering from composite logs, few core data and available internal log data or via the NLOG portal. A more localized, though detailed, petrophysical analysis and correlation of the RBSM was also part of this process, using only log data of the P06 offshore block (GR, sonic, density-neutron porosity). Every well was subsequently grouped based on their dominant lithological character. In this context, purple colour was used to describe dominant anhydritic, massive claystone-mudstone facies while brown colour for dolomitic, laminated, silty claystone or shale, slightly anhydritic and yellow colour for sandy/silty claystone to siltstone, non anhydritic facies. Wells with RBSM completely absent were painted black and interpreted as part of the Winterton High, located in the western margin of the study area (Fig. 6), while wells with RBSM partially eroded were painted grey and interpreted as the Winterton Platform around the paleo-high. As far as the UK offshore wells are concerned, the same lithological distinction was performed using the total sandstone, siltstone or anhydrite content within the RBSM, displayed in the NSTA database. As a result, wells with more than 15%

of sandstone were coloured yellow and wells with more than 10% anhydrite were coloured purple. All the rest silty claystone facies were coloured brown, in line with the NL wells colour scale.

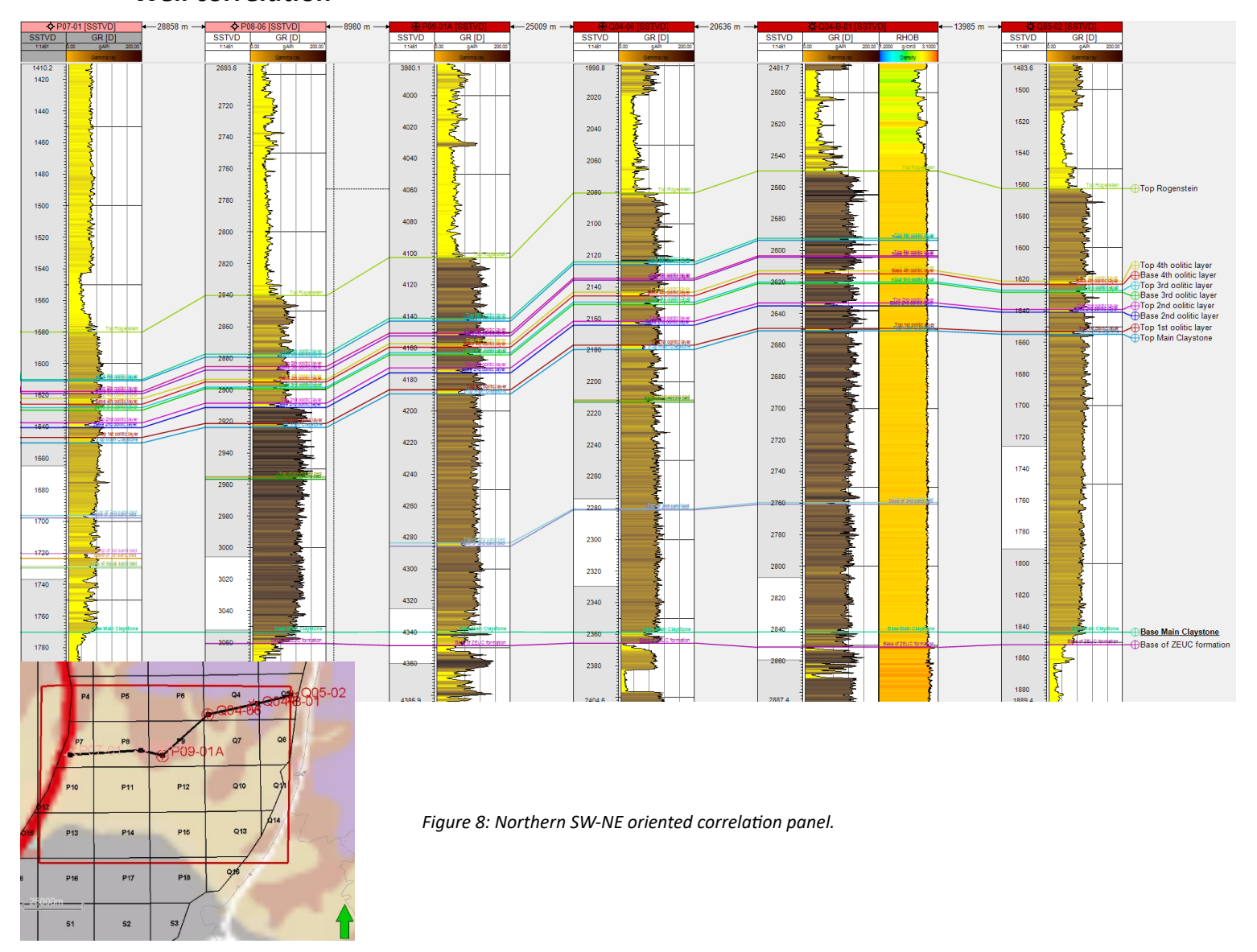
The facies distribution map derived by this process, paved the way for the development of an overall Gross Depositional Environment (GDE) Map specifically for the RBSM in and around the area of interest using QGIS. Moreover, the sand-prone facies presence as well as the presence of the Nederweert Formation (RBSN) stratigraphically below the RBSM, helped infer the dominant fluvial sediment transport direction during deposition.

The sealing capacity evaluation initiated using existing structural data of five depleted fields in the study area, available through the NLOG portal. The depth maps of the top of its structure revealed its potential size and maximum height, measured from the base (of the closure) up to the crest. This height, considering that its field used be utterly filled (filled to spill), equals the maximum column height of CO₂ that can be stored and reveals the minimum sealing capacity (in meters) that the top sealing unit can sustain. Subsequently, research for publicly available or internal lab measurements on the sealing capacity of the RBSM generated only three data points of Mercury Injection Tests (MIT), namely in well P11-04 (offshore) inside the area of interest, the well AMS-01 (onshore) close to the area of interest and a final confidential measurement in the L07 offshore block (further north of the study area). These measurements revealed the potential maximum sealing capacity of the formation in the microscale. In the well AMS-01 where no sealing capacity calculation in meters was available in the lab report, a manual calculation was executed under this study based on the raw data retrieved during the Mercury Injection Test and given mathematical equations typically used for derivation of the CO₂ column heights (Appendix B). The GDE map integrated with the sealing capacity findings facilitated the construction of a gross RBSM sealing capacity map of the study area.

Finally, sonic logs from the entire area of interest were analysed in order to identify any signs of overpressures within the RBSM. A typical trend of decreasing sonic velocity with depth is usually a clear indicator of overpressure, from trapped fluids within the unit during burial. Based on the recently published GEODE atlas (Kortekaas et al. 2023), generally not high overpressures were expected in the study area as the old age of the formation has contributed significantly to (slowly) equilibrate any internal fluid pressures until the present day. However, any signs of overpressures would prove and boost the effectiveness of the sealing formation. The analysis identified evidence of overpressure in at least two wells, namely the Q10-06 and 53_14-1.

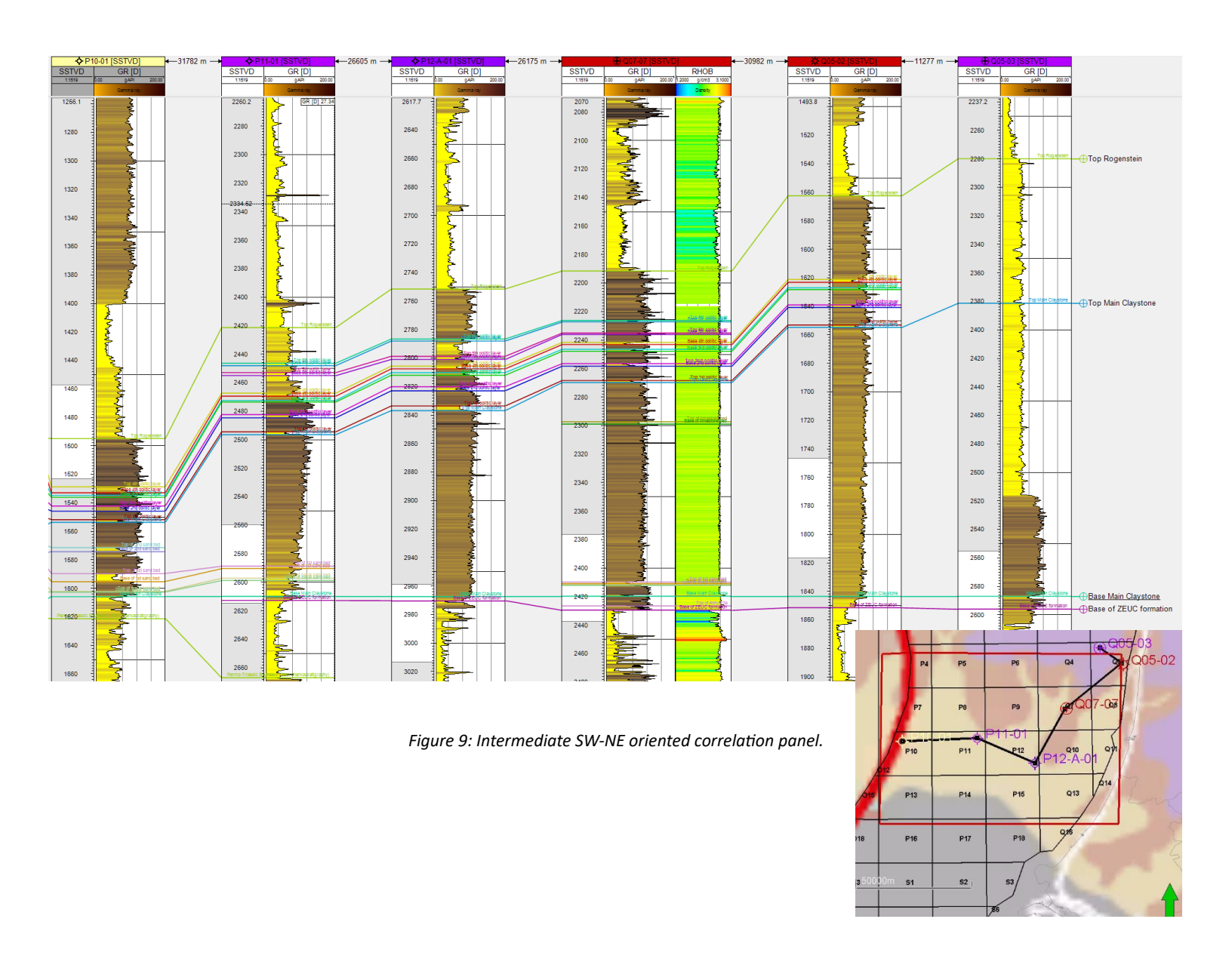
Structural analysis

Well correlation



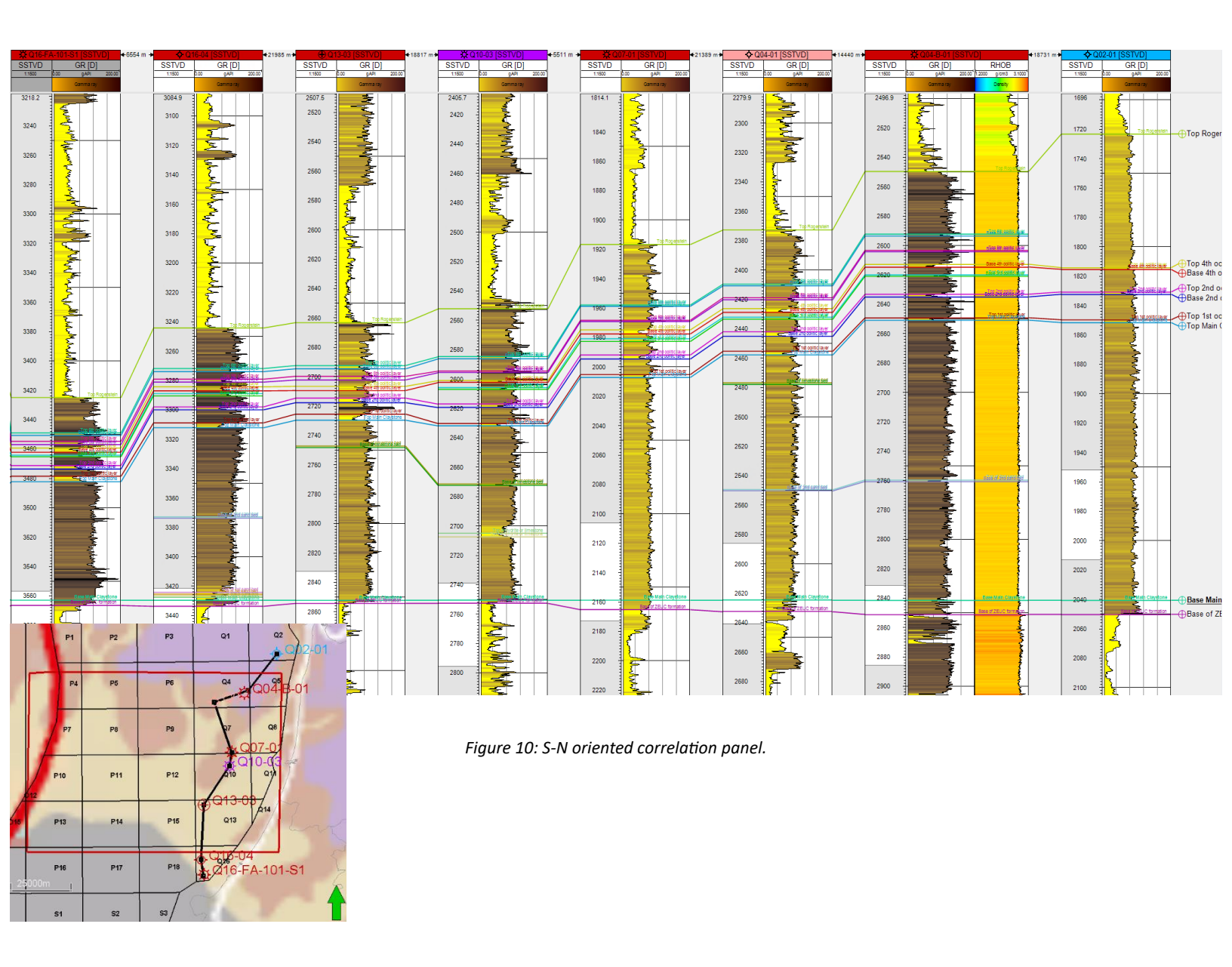
Starting from the bottom, the base of the ZEUC has been easily identified, traced across most of the wells in the study area, by a sharp drop in GR logs accompanied by a sudden increase in density, accredited to the presence of a (relatively thin) pure anhydrite horizon (Fig. 8). The top of ZEUC, representing also the base of the RBSM, is also characterized by a substantial drop in GR without significant density change though, which reflects a sand-rich interval. Higher in the succession, the top of RBSM is picked at the first sharp GR low caused by the basal oolitic limestone interval of the RBSR while the Lower Bunter succession ends at the first sandstone layer of the overlying Volpriehausen formation. Furthermore, in only few wells, P10-01 and P11-01 in figure 9, the Permo-Triassic boundary has been recognised several meters below the base of the RBSM, based on a chemo-stratigraphic study conducted

in SW P-blocks, accessed through NLOG. The latter suggested that the Permo-Triassic litho-stratigraphic and chrono-stratigraphic boundaries do not really coincide.



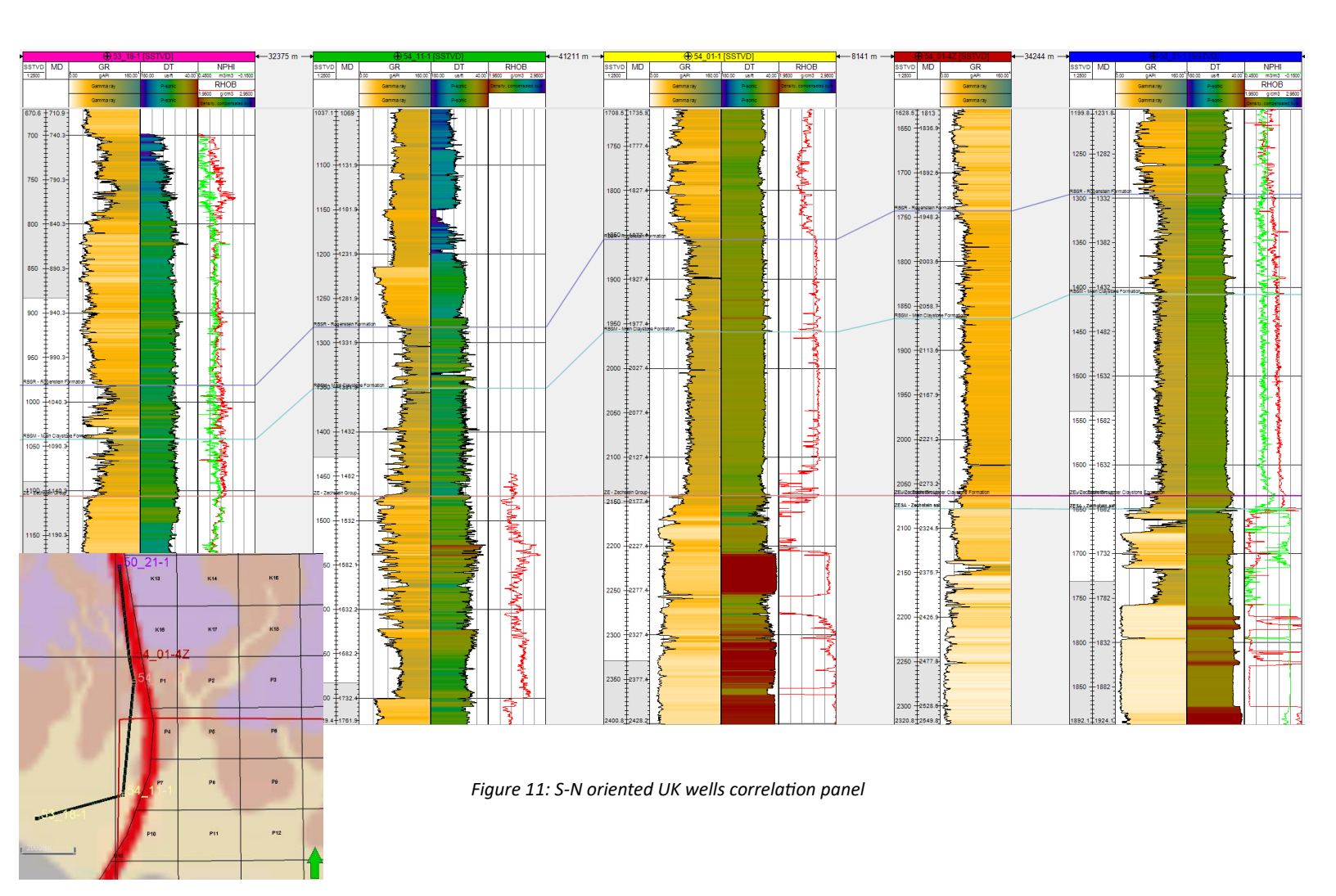
The Lower Bunter succession exhibits an extremely consistent, homogeneous log character characterised by high GR, occasionally exhibiting a slight or clear fining upward GR trend. This trend only pauses at its sandy base and top, as well as at the very distinct, easily correlatable oolitic limestone interbeds of the RBSR, extending across several kilometres. All correlation panels, flattened at the base of RBSM, present almost identical GR patterns standing out in well logs. The only significant irregularity is related to the total thickness of the formation which steadily increases towards the NE and generally N of the study area (Fig. 8-11). Notably towards the SW margin of the study area, especially in wells P07-01, P10-01, P11-01 of figures 8-9, the sand rich RBSM character is prominent, projecting only in that particular region, situated between the Winterton High and London Brabant Massif (Fig. 6). The rest, minor interbeds

traced within the RBSM (Fig. 8-10) occur only locally representing either oolitic sandstone/limestone facies or anhydrite rich horizons.



Well correlation through the UK dataset, also, revealed similar log patterns within the Lower Bunter (Fig. 11). Not only the total thickness consistently rises towards the N, as in the Dutch part, but the sand-rich RBSM character, recognised in the SW margin, resumes in the UK part. Combining GR and Sonic transit time (DT), as well as Neutron porosity with Density logs, the homogeneous RBSM character is illustrated with few minor but distinct irregularities pinching out (Fig. 11). These include the same oolitic facies at base of the RBSR, standing out in every well together with the sand rich facies at the base of RBSM through the wells 53_18-1 and 54_11-1, which quickly fade away further to the North (Fig. 11). A slight to more profound fining upward GR trend can be recognised in RBSM, as along the well sections of the Dutch part, indicating a steady decrease in depositional energy towards shallower successions. This

regime gradually reverses, within the RBSR, to higher energy deposits represented by the oolitic facies across the entire upper part of the Lower Bunter succession.



The prominent, but gradual, thickness increase of the sequence towards the North of the study area can most likely be attributed to the early Triassic paleogeography (Fig. 4-5), as tectonic activity in general postdates deposition. The ephemeral lake's centre and simultaneously its deepest part was located in the northern Dutch offshore and onshore, where the thickness of the succession is expected to reach its maximum. In such a depositional setting the lake's margins, representing the shallowest parts of the paleo-lake, together with the flood plain surrounding the lake are expected to host thinner succession and gradually rise towards the centre, trend apparent in the study area. Additional correlation panels can be found in the Appendix C.

Thickness maps

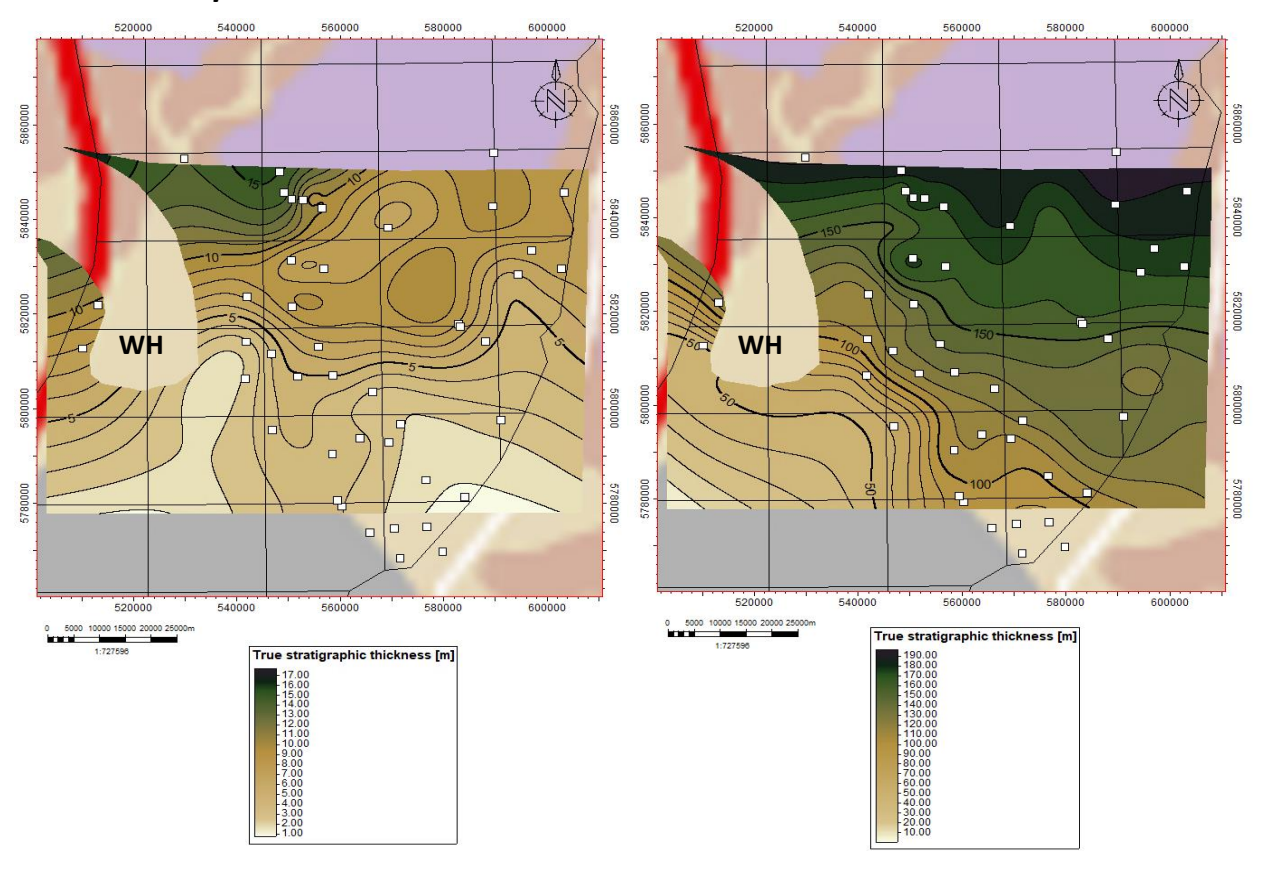


Figure 12: Thickness maps of ZEUC (left) and RBSM (right) formations. They show the present day thickness reduced by the Cimmerian erosion. The initial thicknesses are expected to have been greater. WH: Winterton high, white square points represent well locations used for derivation of the thickness maps, wells drilled within the Winterton High have been excluded as no late Permian or early Triassic succession is present. Namely wells P04-01, P08-01, P10-04, P11-05, P11-10 and 53_10-01 (UK well) have been excluded.

In the western side of the study area, the entire Triassic (and partly the late Permian-Zechstein) succession is absent, as a result of erosion during the development of the Winterton structural High in the early Cretaceous. The area few kilometres around the structural high represents the Winterton platform and is defined by partially eroded RBSM, with RBSR usually completely eroded away. The ZEUC formation's thickness ranges from almost negligible in the southern part up to 15m in the northwestern margin (Fig. 12, left). In the central part of the study area, is measured typically between 5 and 10m. Particularly in the northern part, the existing NLOG interpretation had highly overestimated the ZEUC thickness based on inconsistent well tops that predicted a thickness above 30m. Based on the new adjusted well tops, ZEUC maximum thickness is at least halved in the area of interest. Furthermore, this relatively thin clay-anhydrite rich unit could not constitute an effective top seal independently as it would be prone to juxtaposition even by minor faults. However, it can successfully reenforce the total sealing effectiveness of the overlying Lower Bunter Subgroup. Particularly enhance the sandy base of the RBSM which lies directly above.

The Main Claystone formation reaches maximum thicknesses of 190m towards the north and northeast. Its thickness progressively decreases towards the south and southwest (Fig. 12, right). The

RBSM generally exhibits thicknesses between 100m and 190m in the study area with a significant shift in the southwestern margin where it plummets below 50m. Following a similar trend but under a slightly lower order of magnitude, the RBSR's thickness typically ranges from 50m in the SW to 150m in the NW (Fig. 13, left). The same in principle northwards, gradual increase in thickness is also evident in RBSR while the total thickness of the entire Lower Bunter succession unfolds even more subtle rise towards ,mainly, the NW (Fig. 13, right). It discloses thicknesses in the order of a 100m in the southwestern margin, around 200m in the central part and exceeds 300m in the northwestern margin.

Thickness maps of the four main oolitic intervals within the RBSR can be found in the Appendix D.

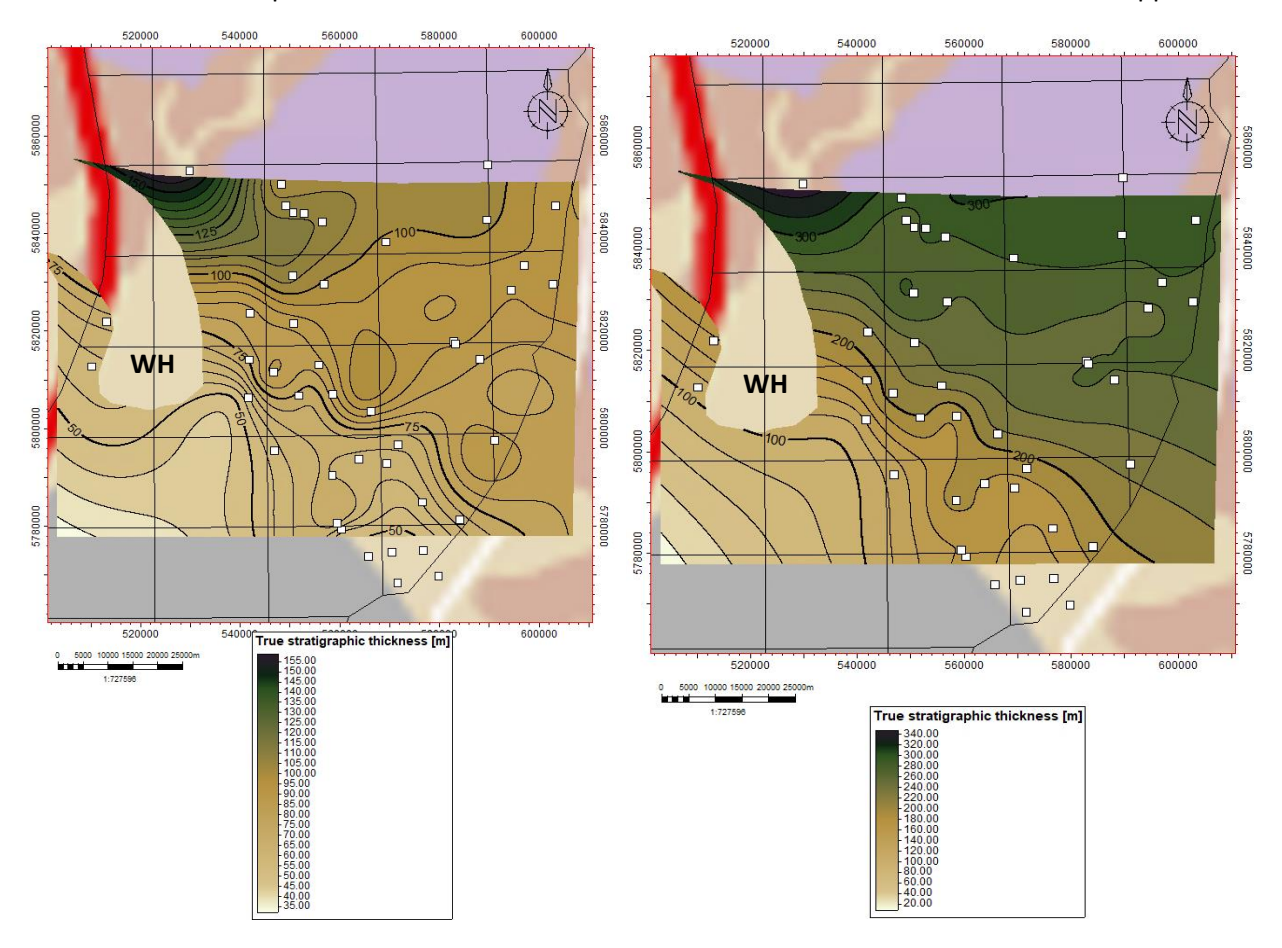


Figure 13: Thickness maps of RBSR (left) and total Lower Bunter (right) formations. They show the present day thickness reduced by the Cimmerian erosion. The initial thicknesses are expected to have been greater. WH: Winterton high, white square points represent well locations used for derivation of the thickness maps, wells drilled within the Winterton High have been excluded as no late Permian or early Triassic succession is present. Namely wells PO4-01, PO8-01, P10-04, P11-05, P11-10 and 53_10-01 (UK well) have been excluded.

Depth maps

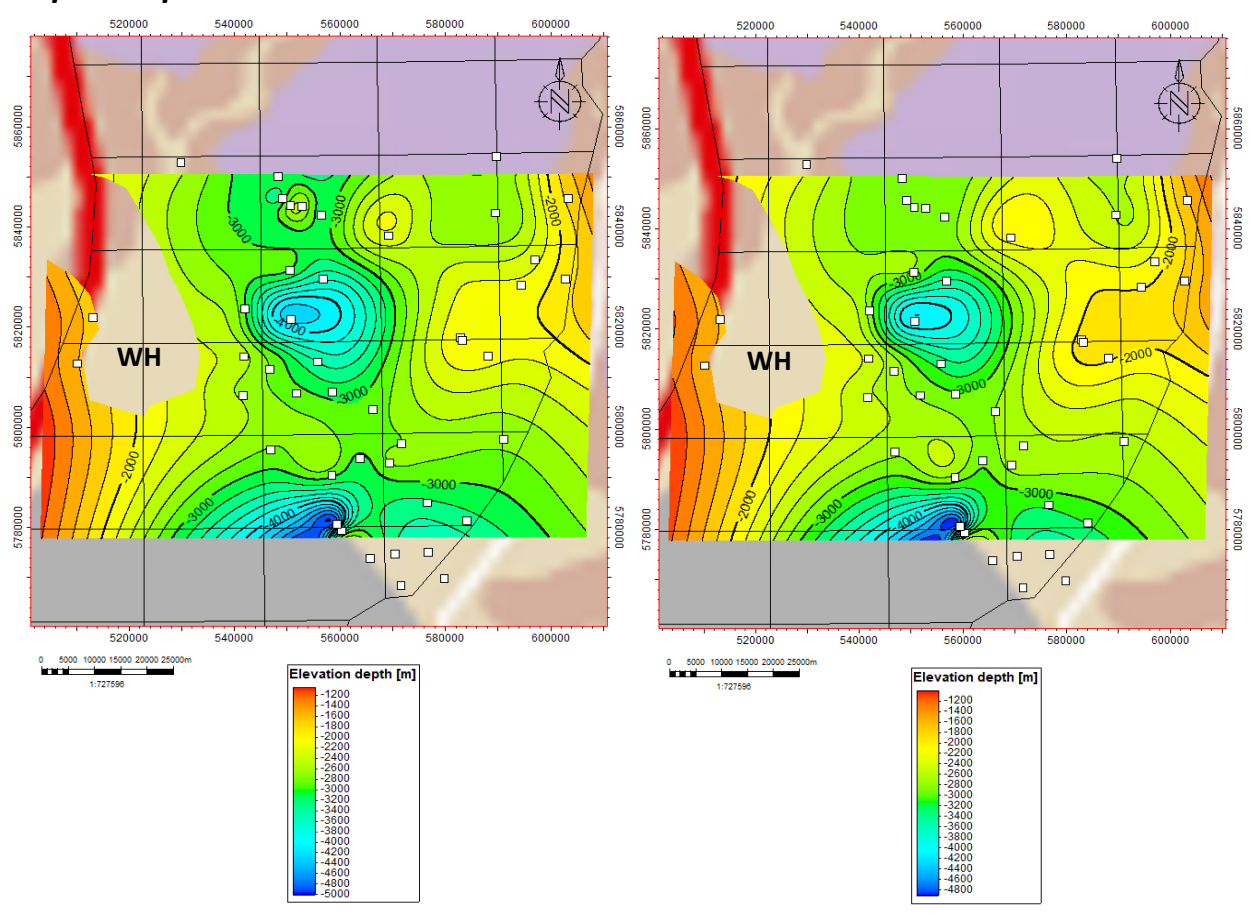


Figure 14: Depth to the top of the RBSM (left) and the top of the RBSR (right) in mTVSS. WH: Winterton high, white square points represent well locations used for derivation of the depth maps.

The RBSM and RBSR depth of occurrence strongly varies in the area of interest (Fig. 14). The Lower Bunter sequence is typically found in the vicinity of 2000-3000m depth, having undergone deep burial during the late Jurassic-early Cretaceous stage of rifting and the development of the West Netherlands-Broad Fourteens Basins in the eastern part of the study area (Fig. 6). The activation of major normal faults, with strong fault throughs, along the margins of both basins has induced even greater burial, exceeding 4000m depths in the central and southern part. Conversely, the western region, close and around the Winterton High, is characterised by shallower depths of occurrence, being part of the relatively shallower Winterton Platform. Finally, the NE side reveals similar shallow depths of occurrence as the SW margin, typically above 2000m, this time attributed to the North-Holland Platform active inversion from the early Cretaceous (Fig. 6).

Compositional analysis

RBSM Lithology

The NNW-SSSE oriented well section of figure 15, flattened at the base of the RBSM, shows the typical petrophysical character of the uppermost Permian-early Triassic succession. Lithologies characterised by extremely low GR, coupled with high Sonic velocity and very low Densities have been recognised as Halite-evaporites whereas units with very low GR, high Sonic but very high Density as Anhydrite. Facies defined by low GR coupled with high Sonic and high Density have been interpreted as sand or silt-rich facies, variably oolitic and lithologies of high GR, moderate Sonic and Density as claystones. Oolitic limestone or sandstone intervals have been recognised by the very low GR and very high Sonic velocity with moderate densities. The distinction between oolitic sandstone or limestone and between massive claystone or silty-claystone is only possible by studying the composite logs from the available well reports.

Starting from the bottom, the sequence is initially characterised by the occurrence of the upper Zechstein salt formations (P06-04A Halite, Fig. 15) which quickly vanish, being replaced by silty to massive claystone facies with thin anhydrite and silty-sandy claystone intercalations (P06-A-02-S1, P06-01, P06-S-01, Fig. 15). These 20-30m thick facies represent, from bottom to top, the Red Salt Clay member, the Anhydrite-Pegmatite member and the ZEUC which act as sealing units, locally, adding up to the primary RBSM sealing formation. However, only the ZEUC extends across most of the study area and effectively contributes to the sealing capacity of the RBSM, with the rest units gradually disappearing towards the southern part. The dashed yellow line in figure 16 represents the boundary of the salt-evaporites occurrence (no salt in the southern part).

Moving up in the stratigraphy, the first approximately 10m of the base of RBSM are characterised by continuous intercalations of silty claystones, siltstones or tight to massive sandstones traced along the entire block. Based, also, on composite logs the basal, tight silt- or sandstones present no visual (very poor) porosity supported by argillaceous or dolomitic matrix and calcareous/dolomitic cement (Appendix E: Core photos). These facies only define the typical sandy base of the formation, however, as the sequence resumes upwards with clay rich facies, of characteristic very high GR values coupled with stabilised, moderate densities and sonic velocities. This typical, fairly homogeneous, clay succession up to the top of RBSM is composed of massive, anhydrite rich claystones towards the northern part of the P06-block and gradually shifts to silty, slightly anhydritic claystones or shales towards the southern margin. The claystone facies are illite/kaolinite bearing with minor chlorite, without evidence of swelling clay minerals (smectites). Heterogeneities within the RBSM include only minor, localised, relatively thin sand sheet intervals, few thin anhydrite or salt horizons and more easily correlatable, oolitic limestone or sandstone facies close to the top of the succession (Fig. 15). These intervals are considered to have limited lateral extent without being interconnected and are generally too rare to form continuous pathways (leak paths) along the RBSM seal unit.

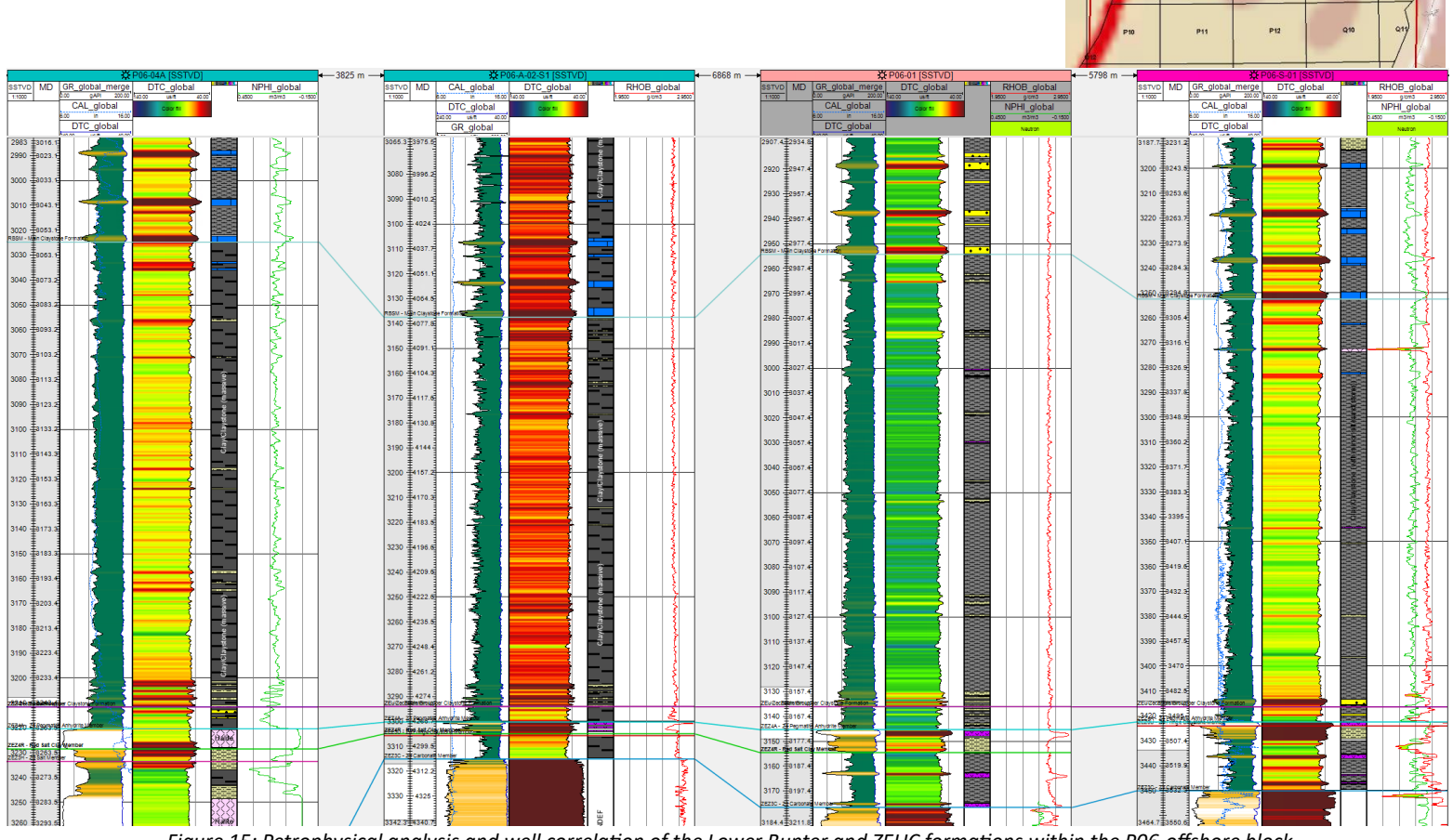


Figure 15: Petrophysical analysis and well correlation of the Lower Bunter and ZEUC formations within the P06-offshore block.

Dark colour: Massive claystone, Grey colour: Silty claystone, Yellow pale colour: Intercalations of silty claystone, siltstone and tight sandstone in the microscale, Yellow bright colour: Massive sandstone (oolitic), Blue colour: Oolitic limestone, Purple colour: Anhydrite, Pink colour: Halite.

Directly at the base of the first major oolitic limestone layer, the RBSR formation initiates with at least four main oolitic facies intersected by similar clay facies as the underlying RBSM. The oolites are generally Fe-calcareous, fine grained, tight, firm to hard, in a very calcareous/micritic matrix with traces of anhydrite. Rarely the lithology of the clay rich successions diverge between RBSR and RBSM, illustrated in the P06-04A well of figure 15. Towards the top of the formation the oolitic facies fade away whereas the clay facies experience a slight coarsening upward trend. The oolitic facies of RBSR can be distinguished by the very low GR followed by sharp sonic velocity increase and occasionally density pick. These intervals stand out in the well log surrounded by the high GR, moderate sonic velocity and density of typical shales/claystones and can be traced across several kilometres.

The integration of all the available (GR, Sonic, Density, Neutron) log data with composite logs in and around the focus area resulted in a regional dominant facies distribution map for the RBSM (Fig. 16). Accordingly, wells P06-04A and P06-A-02-S1 of figure 15 have been classified as massive, anhydritic claystone (purple in figure 16) while the wells P06-01 and P06-S-01 as silty, slightly anhydritic claystone or shale (brown in figure 16).

Massive, rich in anhydrite claystone facies dominate the northeastern corner of the area of interest extending north and northwest-wards to the PO2-, PO1-, K18-NL and 50-UK offshore blocks (Fig. 16). Conversely, the central part and southeastern corner of the area of interest is almost completely covered by silty, slightly anhydritic claystone/shale facies. In contrast, the entire western part has been impacted by the Winterton High, which has caused the complete erosion of the early Triassic succession and the partial erosion of RBSM on its flanks. The wells characterised by partially eroded RBSM host relatively thin, sand-silt rich siltstone to claystone facies overwhelmed by the effects of leaching closer to the structural unconformity (Cimmerian). Finally, sandy/silty claystone prevails only in the western side of the Winterton High (UK offshore) and in the southeastern NL onshore, close to the Roer Valley Graben. Additionally, in both locations the Nederweert sandstone (RBSN) is present and underlies the RBSM.

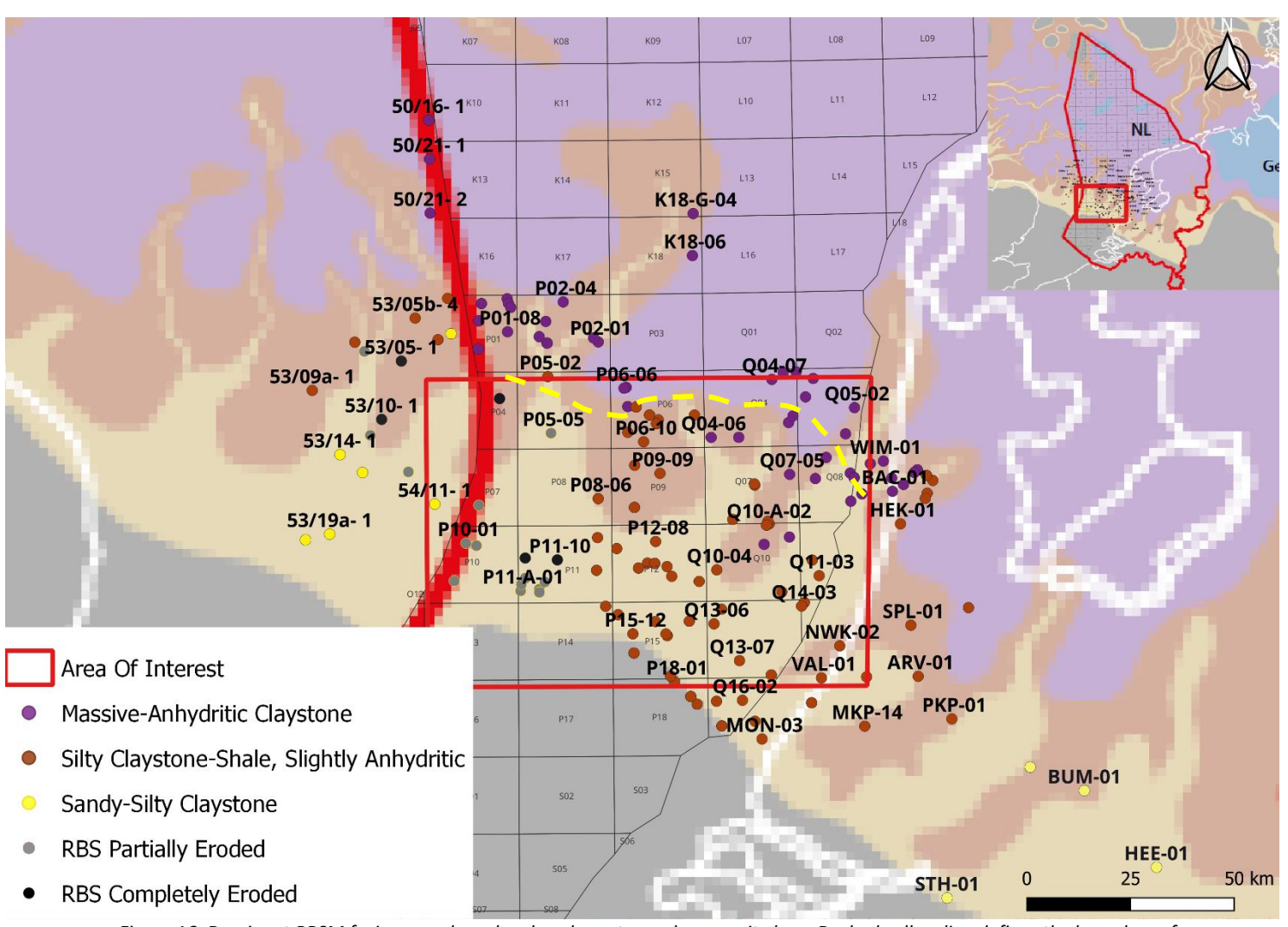


Figure 16: Dominant RBSM facies map, based on log character and composite logs. Dashed yellow line defines the boundary of Zechstein evaporites occurrence (no evaporites south of the boundary).

Porosity/Permeability plots

Core data from both the RBSM and RBSR are scarce in the NL offshore. In few offshore wells where RBSM core data have been retrieved, namely P10-01 and P11-04, are mostly representative only of the sandy base of the formation (orange and green data points, Fig. 17). In particular, Poro./Perm. measurements within RBSM in P11-04 well have yielded relatively high porosities (green data points, Fig. 17) for a clay unit, attributed to the location of the well close to the Winterton High and the associated weathering effects. Moreover, measurements in the well P10-01 were taken from an oolitic sand rich interval within the RBSM, justifying the high porosities and horizontal permeabilities (orange data points and trend line, Fig. 17) which show a typical, though very slight trend of Poro./Perm. loss with depth due to compaction (shallower data point is the one with the larger porosity).

RBSM PORO-PERM PLOT: Output Description of Market and analy base of formation in the first and analy base of formation in Tight color breaktone. Fight color breaktone Output Description of Market and analy base of formation in Tight and the formation in Tight

Figure 17: Porosity/Horizontal Permeability plot of core plugs within the RBSM.

In the onshore NL, three wells with RBSM core measurements, BUM-01, EVD-01 and AMS-01, are available and represent the true clay rich core of the formation (Fig. 17). Also, extensive core measurements from the well WYK-32 are available but not selected for the current study due to its distance from the area of interest. Plotting all the Poro./Perm. data from the three wells reveals a typical cloud dataset which usually characterises shale/claystone formations (blue data points, Fig. 17). This dominant facies inside the RBSM exhibit generally low porosities, below 5%, accompanied with relatively low to very low horizontal permeabilities, lower than 0.7mD with many points lower than the permeability measuring limit in the Lab (usually 0.01mD).

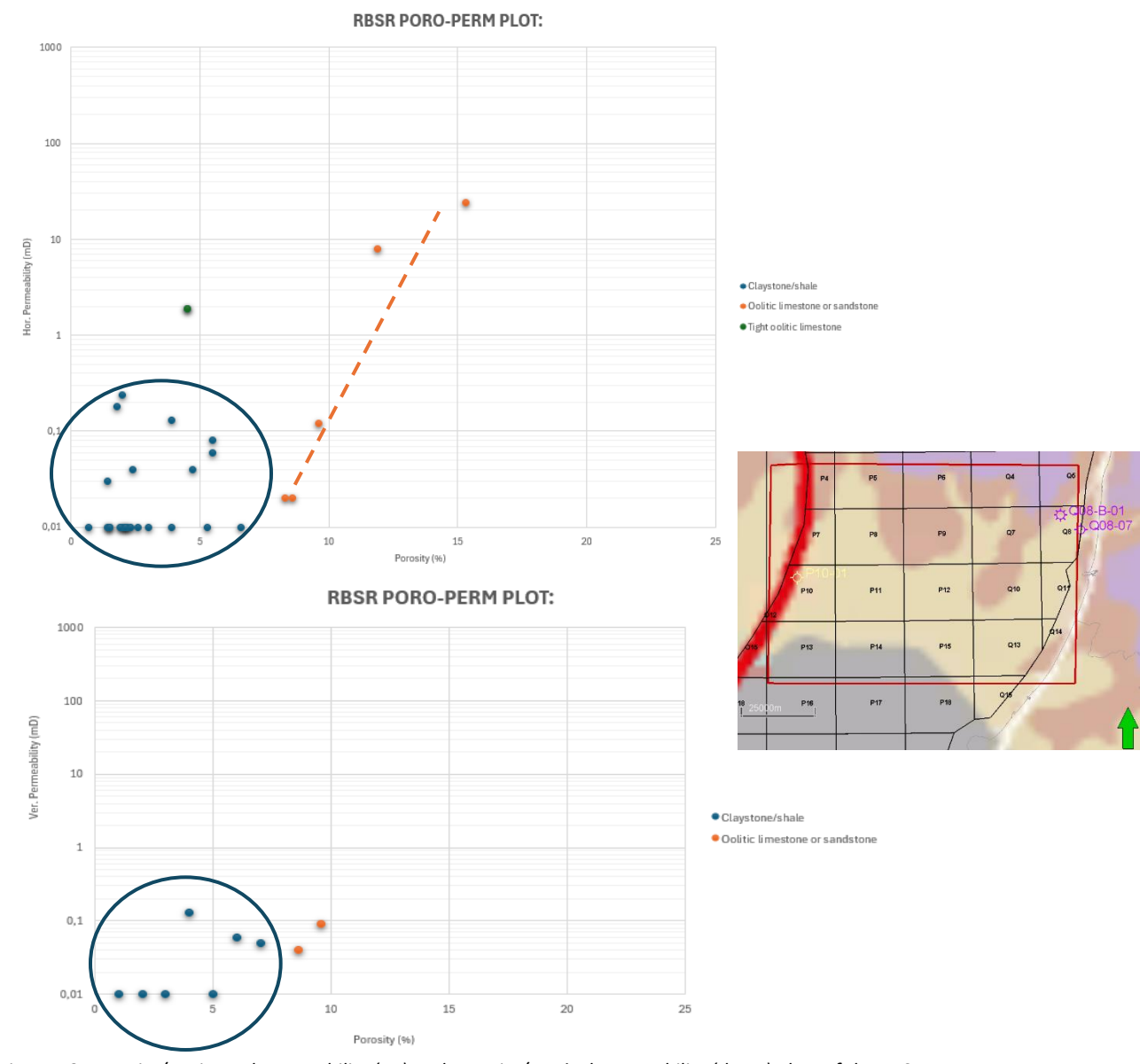


Figure 18: Porosity/Horizontal Permeability (up) and Porosity/Vertical Permeability (down) plots of the RBSR.

Similar to the RBSM, core measurements from the RBSR were taken only from three offshore NL wells, P10-01, Q08-07 and Q08-B-01 (Fig. 18). Onshore wells STH-01 and WYK-32 were excluded being too distal from the study area. Plots of Poro./Perm., both horizontal and vertical permeability, reveal similar cloud dataset for the clay/shale facies, with lower than 5% porosities and permeabilities of the order of 0.1mD and lower (blue data points, Fig. 18). The oolitic facies, again, show higher porosities and permeabilities with a slight decreasing trend with depth.

Evidently, more core measurements for both formations from different depths and locations would result in a more profound study and detailed picture of the porosity and permeability trends with depth as well as with the depositional environment or the effect of leaching from structural unconformities.

Sealing capacity evaluation

Structural maps of known fields

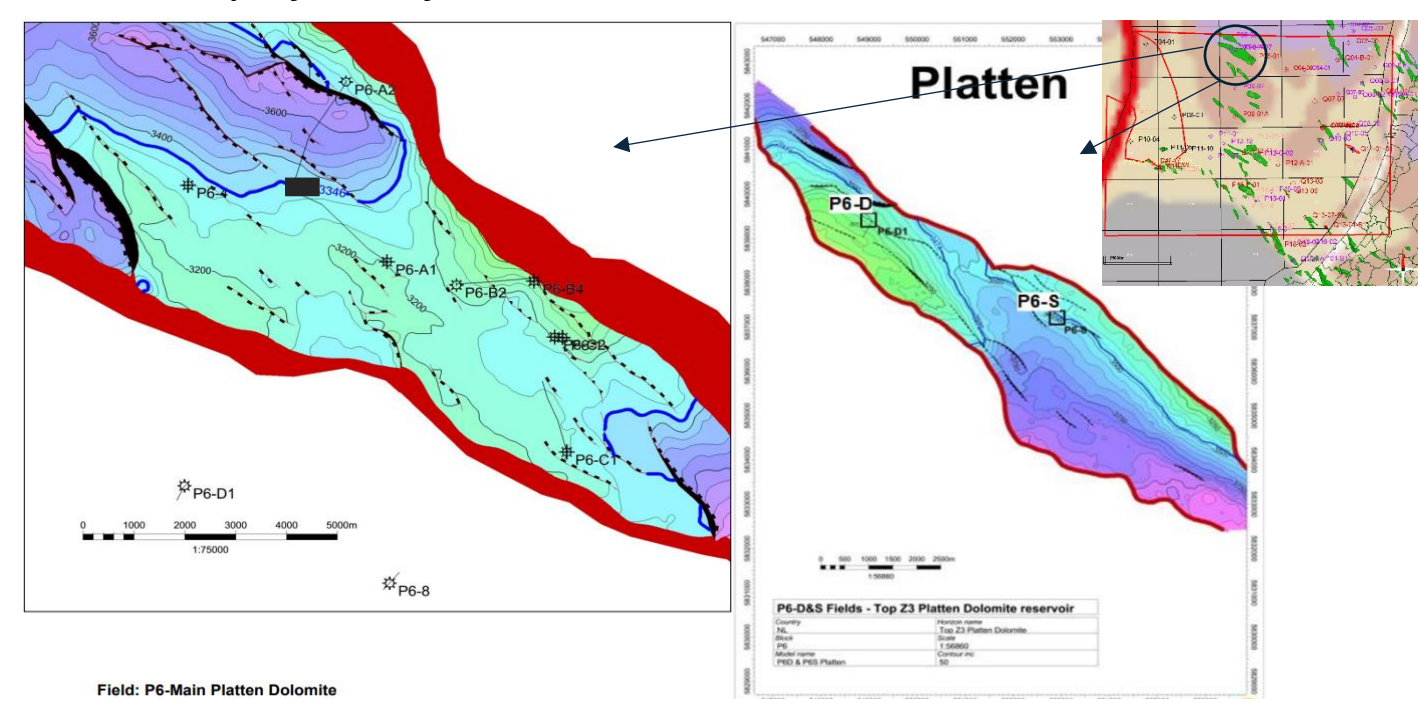


Figure 19: Depth maps of Z3 Platten Dolomite reservoir in P06-Main and minor depleted fields (source: NLOG). Blue contour line represents the base of the structure (spill point, source: NLOG).

A first order estimation of the RBSM's sealing capacity (in meters) has been withdrawn by known depleted fields in the study area. Studying the depth map of the largest structure in the area of interest P06-Main field (Fig. 19, left), its maximum height is measured, counting the contour lines from the bluebase line up to the crest, at 346m. Following the same process for the P06-Minor fields, P06-S reaches a maximum height of 324m while the P06-D exceeds 425m (Fig. 19, right). This potentially indicates that the sealing formation on top (RBSM) could sustain a CO_2 column height of at least 400m (and more) and is only limited by the dimensions-size of the structure. Thus, the upper limit for the sealing capacity of RBSM in this particular region is likely more than 425m, the highest point of all the structures.

An additional significant field situated closer to the centre of the study area is the Q10-A (Fig. 20, left). In this region, the total height of the structure is measured at 203m, enough to maintain an order of magnitude lower amounts of CO₂ than the P06 fields but its limited by the total size of the structure not the top seal effectiveness. This is because in both regions the RBSM is composed of the same dominant facies (Fig. 16) and showcase similar total thicknesses without any effects of leaching from structural unconformities, so its sealing capacity is expected to remain constant. One last known field in the study area is located in the P11-block (Fig. 21), where the RBSM has been partially eroded and only 15m of the formation remain. The total height of the structure reach its maximum at 165m, however the CO₂ column height that could be stored is largely limited by the top seal effectiveness in this part, possibly below 100m. The formation has been heavily weathered and its thickness is insufficient for safe sealing on top, mainly

due to the Winterton's High development during the early Cretaceous. In this particular region, the shallower early Cretaceous Vlieland Claystone formation, which lies directly on top of RBSM, is likely effective in sealing on top for CO_2 rather than the Main Claystone.

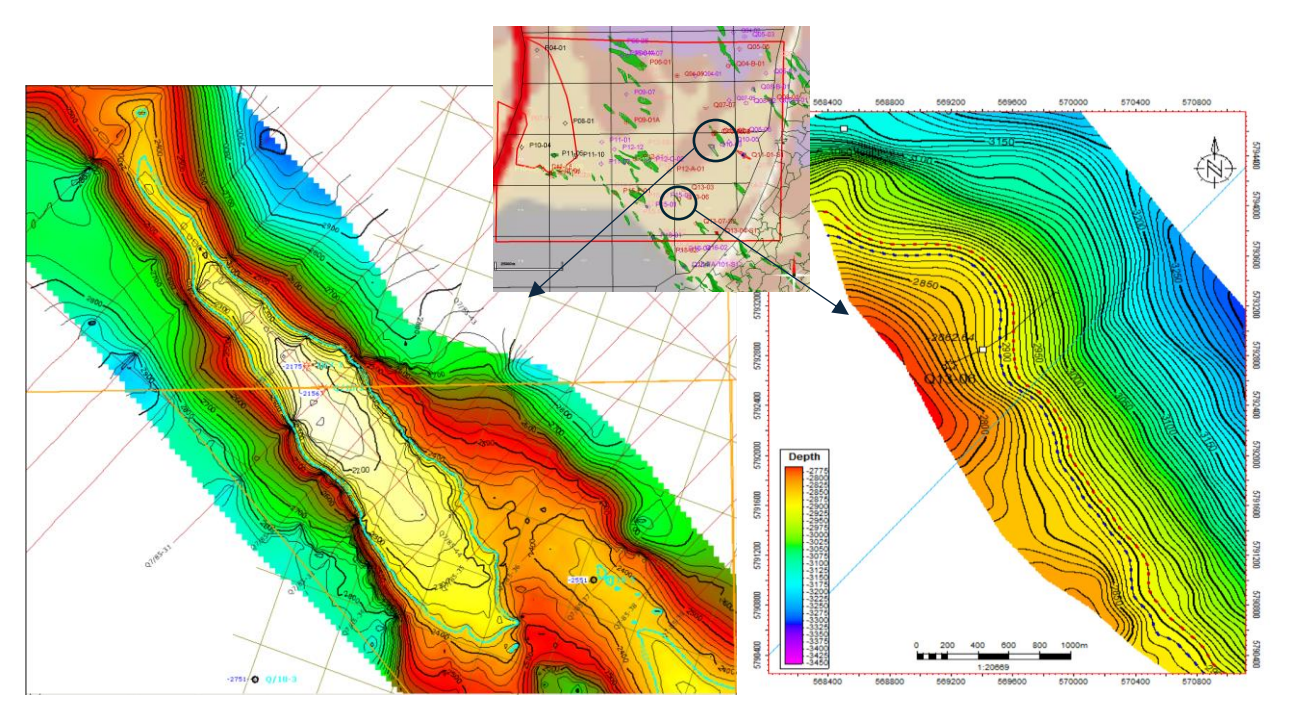


Figure 20: Depth maps of Top Z2 (Stassfurt) Formation in Q10-A field (left) and Top Z1 formation in Q13-FC field (right). Blue contour line represents the base of the structure (spill point, source: NLOG).

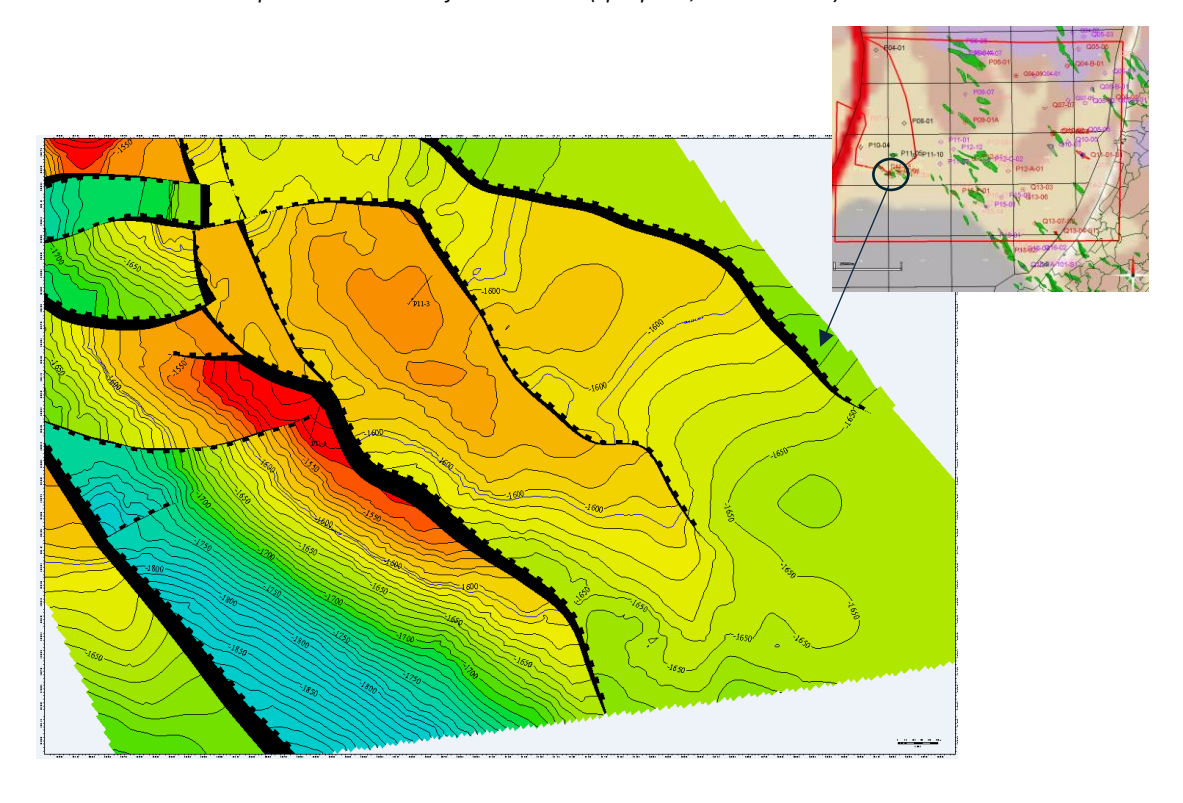


Figure 21: Depth map of the Base Vlieland formation, P11b De Ruyter field. Here the Vlieland Formation forms the top seal for various underlying accumulations. Blue contour line represents the base of the structure (spill point, source: NLOG).

Sealing capacity measurements (MITs)

Regarding the existing sealing capacity direct lab measurements of the RBSM using Mercury Injection Tests (MIT), there are three available tests performed in both offshore and onshore wells, presented in figure 22. The first and only one inside the study area measurement in the P11-04 well exhibits max. sealing capacities for CO₂ ranging from 45m to 145m depending on the lithology and the level of stratification. Massive-blocky claystone facies hosts the highest sealing capacity as a result of the highest threshold pressure it presents for mercury to invade its pore spaces. The measurement is generally in line with the expected only minor sealing potential of the RBSM in this region, affected by leaching effects of the proximal structural unconformity. Another measurement is included in the recent AMS-01 onshore well, situated few kilometres outside the area of interest, where the CO₂ max. sealing capacity of the RBSM is calculated between 360m and 465m. As reported in the P06-Main field (Fig. 19), the formation is capable of supporting CO₂ columns of at least 425m and now based on the MIT it has the potential to reach up to 465m. The final sealing capacity information is retrieved through internal research, from the CO₂ storage department of the EBN B.V., focused on the L07 offshore block (Fig. 22). Their results are confidential thus, it can only be stated here that the max. sealing capacity of the RBSM substantially increases towards the northern NL offshore.

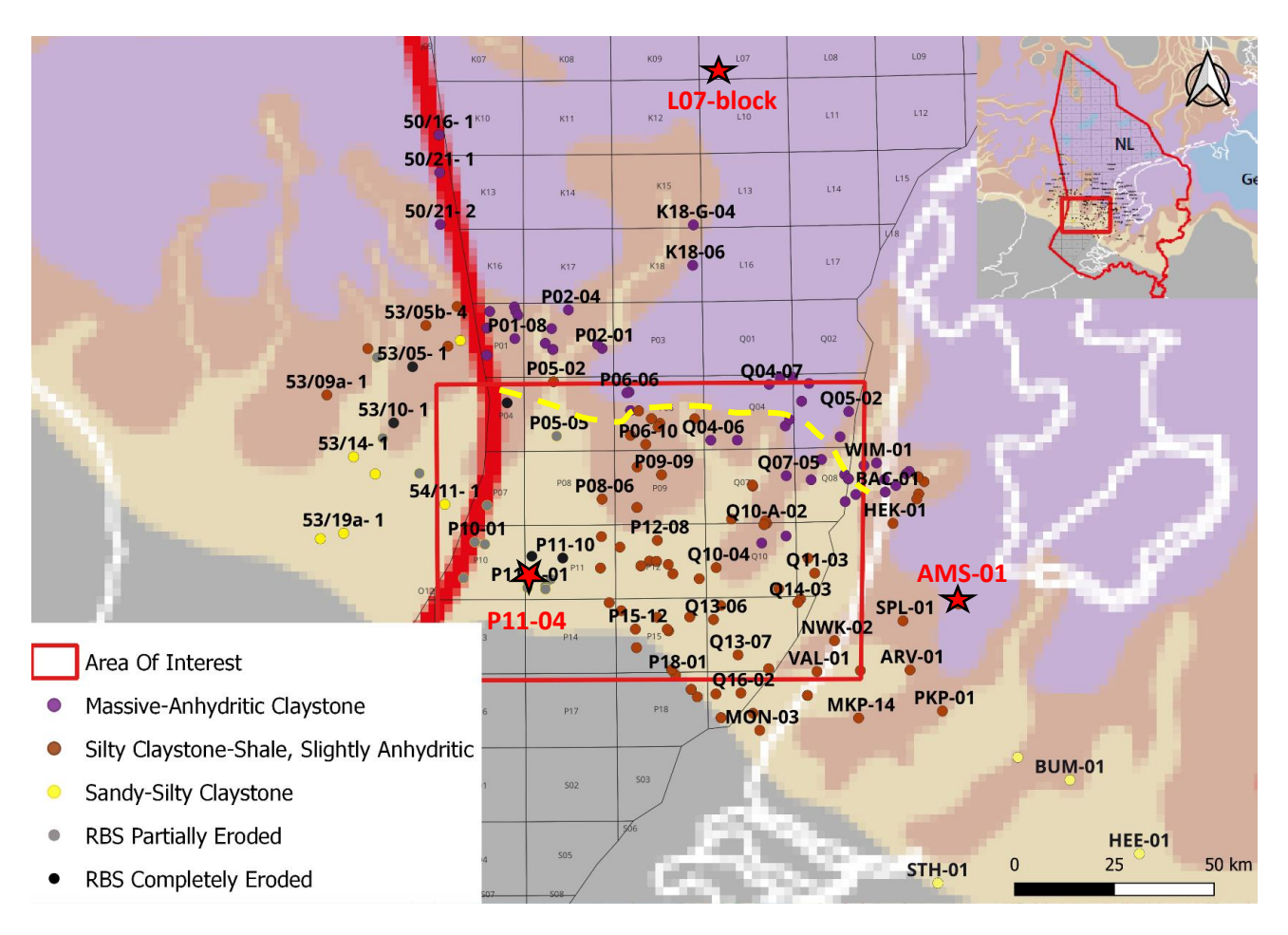
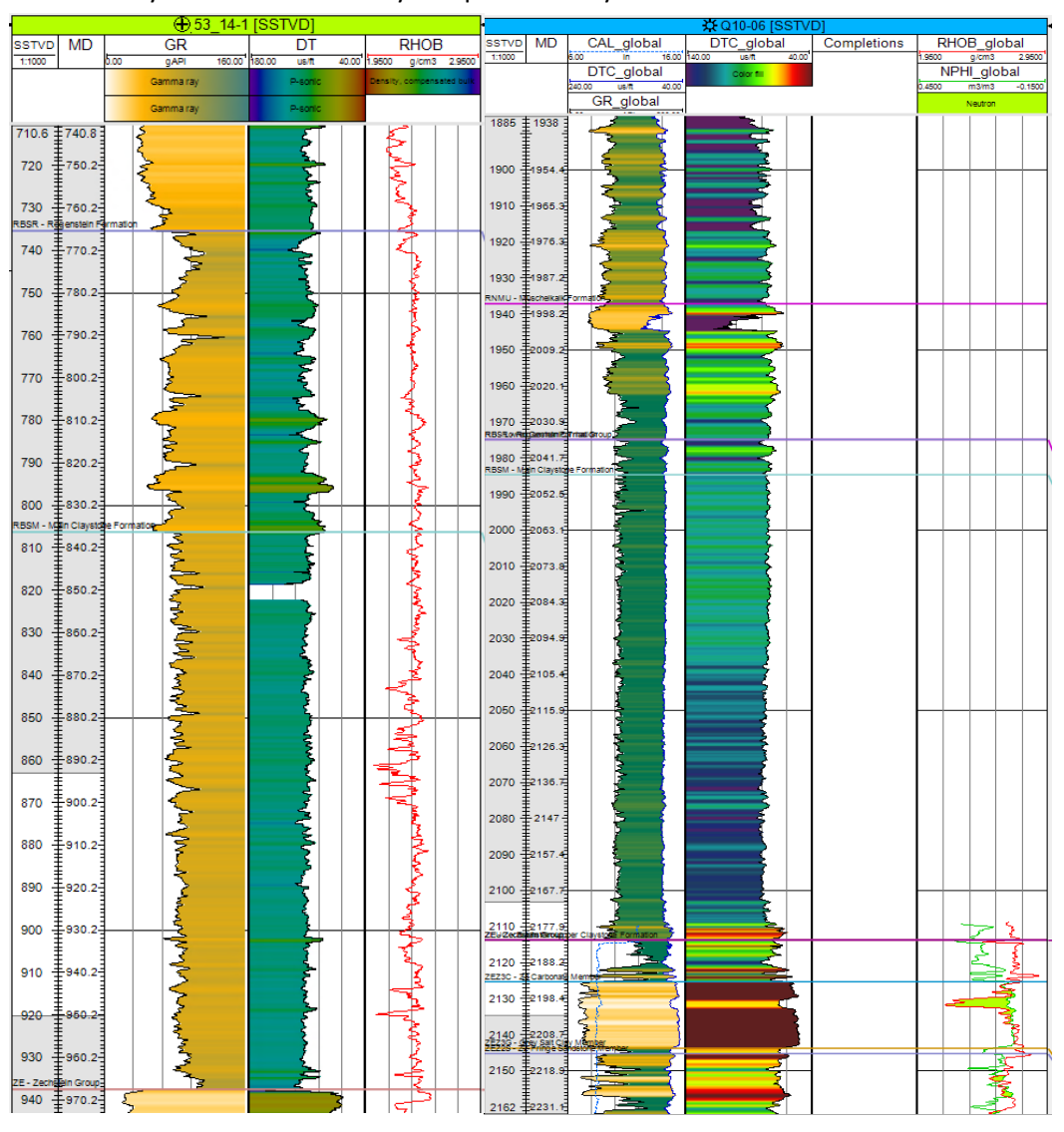


Figure 22: Dominant RBSM facies map with the three data points of sealing capacity measurements, represented by red stars.

Dashed yellow line defines the boundary of Zechstein evaporites occurrence (no evaporites south of the boundary).

Overpressure analysis

Overall, no significant early Triassic overpressure build up was expected in the region. Any initial overpressures due to rapid deposition and burial believed to have already been equilibrated up to the present day. Based on the recently published annotated Triassic play maps by Kortekaas et. al. (2023), overpressures are generally expected only towards the northern NL offshore and the northeastern NL onshore (south of the Groningen field). Furthermore, overpressure measurements are sparse in the area of interest for the RBSM. The only overpressure data available are located in P12-C-02-S2 and P09-09-S1 wells (and STH-01 onshore well outside the study area) both exhibiting negative values (from -18 to -45 bar) meaning that the formation is locally under-pressured (Appendix G). This could be a result of dehydration due to deep burial and compaction or even hydraulic disconnection from nearby aquifers or reservoirs caused by the formation's very low permeability.



However, even minor indicators of overpressures would boost the current research of the Main Claystone formation seal effectiveness in the study region. Thus, the analysis incorporated all the UK and NL wells in the area of interest with emphasis on their sonic logs in an attempt to identify any trends with depth.

The vast majority of the wells inside the area of interest have not revealed any significant sonic log trends. However, the first example of an only minor sign of overpressure includes the UK well 53_14-1 (its location can be found in figures 16 or 22). The DT log, which translates to the Transit time of the sonic waves, within the Main Claystone exhibits a very slight increase with depth (Fig. 23, left). This increase of the transit time implies an associated decrease in sonic velocity with depth which can potentially be attributed to trapped fluids inside the formation, leading to overpressures. On the contrary, lithological factors such as the GR trend within RBSM showing a fining downwards trend, could also cause the observed decreasing sonic velocity trend with depth. However, finer grained lithologies (claystones) towards the base are generally expected to be denser than the coarser close to the top (siltstones). Denser materials would boost the sonic velocity not hinder it as observed (Fig. 23, left). So, excluding the impact of lithology, the most probable answer is that effectively trapped fluids within the formation (especially the base) have led to the above sonic velocity behaviour.

The following example incorporates a similar but more pronounced sonic log trend in the offshore NL well Q10-06 (Fig. 23, right). The transit time gradually rises in depth, so the sonic velocity decreases, while no significant lithology change can be distinguished from the GR log. This is clearly a result of trapped fluids and indicates that the formation acts like a seal on top in the Q10 region, where known reservoirs for effective CO_2 storage are present (Fig. 20, left).

Both overpressure indicators, in correlation with all the other findings, strengthen the sealing potential of the RBSM in the southern NL offshore. Particularly, the potential in the central and eastern part of the study area is expected to be substantial. Generally, the effectiveness is expected to steadily increase towards the north.

Discussion

Gross Depositional Environment (GDE) map of the RBSM

Utilizing the dominant facies map of the RBSM (Fig. 16) to infer an overall depositional setting, a Gross Depositional Environment map was constructed for the entire southern Dutch offshore during the early Triassic (and onshore, Fig. 24). The southern region from the P14-P15 offshore blocks is completely covered by the London Brabant Massif orogenetic complex which extends several kilometres into the UK and in the opposing direction into the southern NL provinces. Any early Triassic deposition has been completely eroded in that region. Initially, the dominant fluvial sediment transport direction was both SW-NE and SE-NW, sourced from both sides of the London Brabant Massif. The Nederweert sandstone formation (RBSN), present also in both sides of the massif (Appendix F), constitutes the alluvial fans development at the base of the orogen providing constant influx of clastic sediments into the basinephemeral lake which was located further to the north. The SE side was marked by the presence of the Roer Valley Graben, active since the Permian, enriching the basin with clastic sediment influx (towards the NW). On the other side, clastic input into the basin (towards the NE) achieved by alluvial fans situated in the UK part of the offshore. An isolated channel has also been identified in the UK offshore which transported fresh fluvial sediments deeper into the basin (Fig. 24). In both the SW and the SE regions the Main Claystone is composed of continuous calcareous/dolomitic sand-, silt- and claystone alternations characteristic of flood plain deposits, surrounding or overlying the sandy alluvial fan deposits of the RBSN.

The alluvial sediments, though, did not expand to such an extent to cover the central part adjacent to the London Brabant Massif. That part, starting from the blocks P15-Q16, as well as the entire central and southeastern part of the area of interest is dominated by slightly deeper, marginal lake facies characterised by calcareous/dolomitic silty claystones or shales with minor anhydrite. The shallow lake facies extend several kilometres both to the SE further into the Dutch mainland and to the NW towards the UK offshore. In the northeastern corner, the marginal deposits start being replaced by deeper lake deposits of the paleo-playa lake centre defined by massive, hard, rich in anhydrite claystone shows. These facies dominate the entire northern part of the study area covering the most part of the central and northern Dutch offshore.

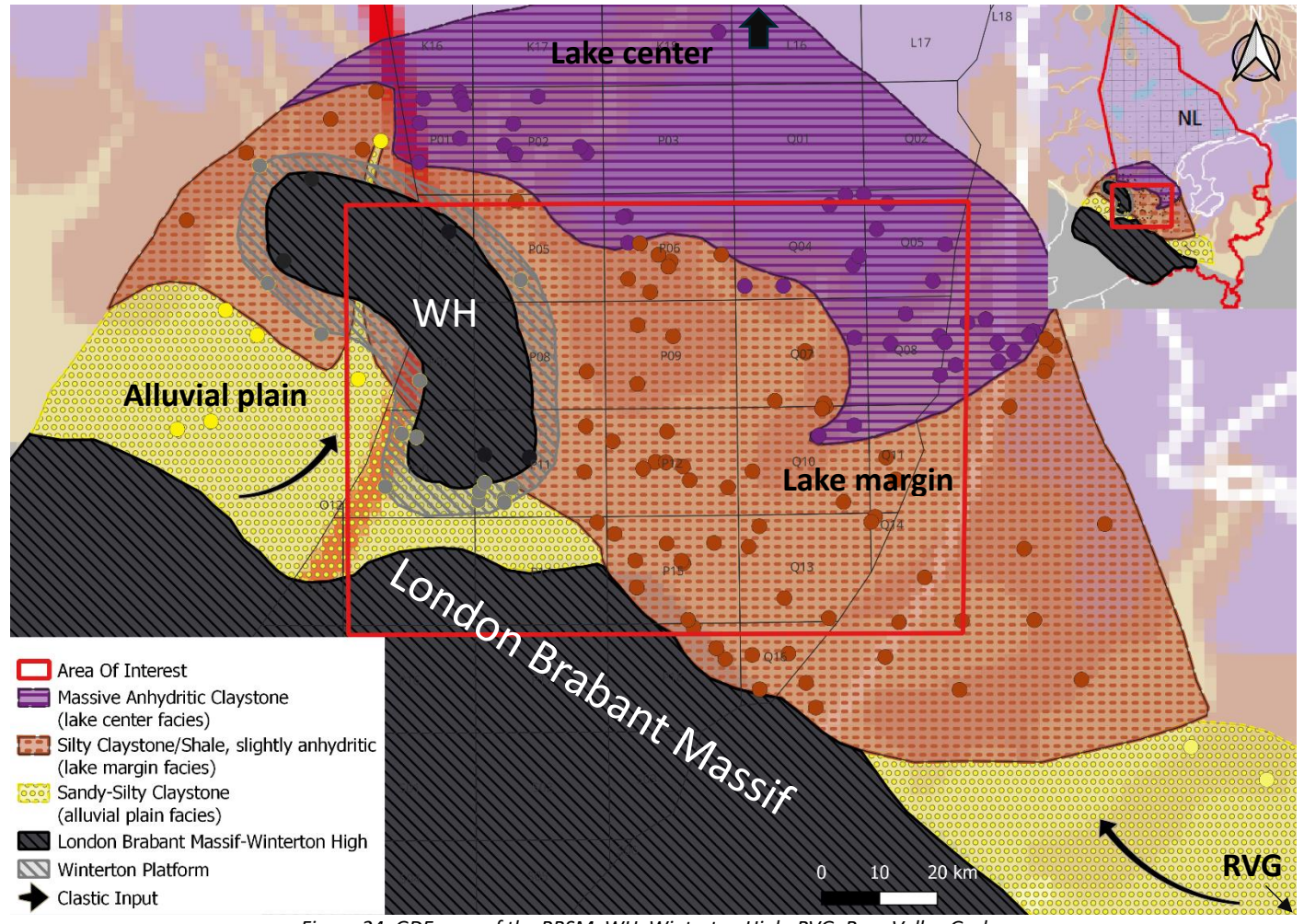


Figure 24: GDE map of the RBSM. WH: Winterton High, RVG: Roer Valley Graben.

Despite the presence of the London-Brabant Massif in the southern part, another highland structure has marked the present day distribution of the RBSM formation. This structure is the Winterton High which developed on the northwestern part during the late Jurassic-early Cretaceous extension phase, postdating the London-Brabant Massif (Fig. 24). Uplift and erosion of the strata within the structural high has led to their complete absence nowadays while around the structural high RBSM has been partially eroded, being part of the shallow water Winterton Platform. Although a much older, Carboniferous, age of the structural high's development has also been proposed (Kombrink et al., 2012), no signs of deposition sourced from the structural high has been recorded within the RBSM. On the occasion that the structural high was present as far as the Carboniferous, alluvial fans represented by sand prone deposits would cover the region around the high and would have transported coarser grained sediments towards the north deeper into the basin. Especially towards the north of the Winterton High, lake margin and centre facies directly dominate the proximity of the high, undermining the above conception.

The GDE map proposed under the current study (Fig. 24) is generally in line with the initial interpretation under Geluk (2005), presented in figure 5. Only few minor differences can be detected regarding the size of the structural high and the lateral extent of the alluvial plain facies in the two opposite

sides of the London Brabant Massif. Although an isolated channel has been identified in the UK offshore, the facies distribution map proposed under McKie and Kilhams (2025), presented in figure 4, appears to be highly unrealistic particularly inside the area of interest. Neither isolated channels have been identified within the study area nor fluvial sandstone facies dominating most of it. Instead, the focus area is dominated in principle by silty claystone/shale deposits being replaced by massive-anhydritic claystone towards the northern part. The latter facies in contradiction to fluvial sandstone facies, although continental in origin, it has been shown that they present substantial sealing capacities attributed to their advanced clay content, level of compaction, stratification and the anhydritic content.

Sealing capacity map and sealing potential of RBSM

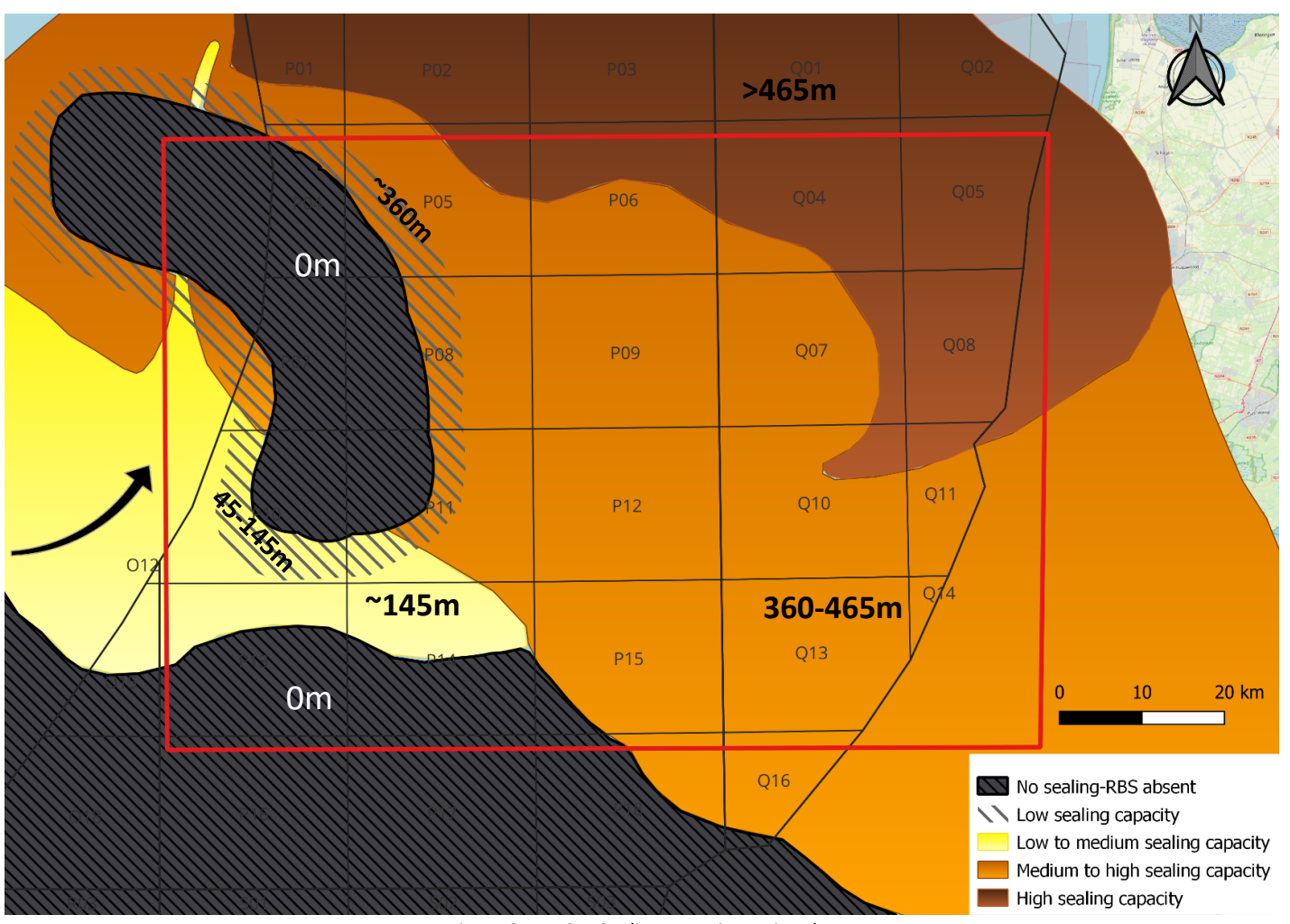


Figure 25: RBSM Sealing capacity regional map.

Based on the findings under this study, a conceptual RBSM sealing capacity map is proposed, controlled mostly by the lithological character and direct sealing capacity measurements (Fig. 25). Excluding the highland regions where the RBSM is absent and shallower formations act as a top seal such as the Vlieland Claystone (Winterton High), limited sealing capacity, 45-145m, carry regions of heavily

weathered and thin RBSM situated mainly in the southwestern side of the Winterton High (P10-P11 blocks). A restricted region covering half of the P13 and P14 blocks as well as a small portion of P10 block could potentially exhibit enhanced seal capacities around 145m. However, not sufficient number of wells is available in that specific area so the risk is still high to safely predict the sealing effectiveness. Evidently, the entire southwestern part of the study area would be advised to be avoided on the grounds that both the top seal has been compromised and the lack of well data increases the uncertainty.

Contrastingly, the central and eastern part of the study area displays significant sealing potential predicted with higher confidence (Fig. 25). The formation is not easily juxtaposed against permeable layers by large fault throughs as its thickness there is substantial (Fig. 12, right). In terms of lithology, the formation is dominated by impermeable, compacted claystones/shales layers relatively rich in illite with minor anhydrite which destroy the total effective porosity/permeability of the sealing formation (Fig. 15-16). Overpressure build up from trapped fluids within the formation in the Q10 block (Fig. 23, right) is an additional strong contributor to the sealing effectiveness in the region. Small scale sealing capacity measurements, at last, indicate a column 360m to 465m high can be safely sustained under the RBSM lithologies while the largest existing structure of the area, the P06-Main field (Fig. 19, left) and the highest structure of 425m, the P06-D field (Fig. 19, right) also use to support comparable column heights. The sealing effectiveness is gradually boosted towards the north and northeast, exceeding 465m sealing capacity, due to the increasing anhydrite content and the rising massive-hard character of the formation closer to the paleo-playa lake's centre (Fig. 25).

Overall, all the available data converge on the very high sealing potential of the Main Claystone regionally, in particular the central and eastern part of the area of interest. Integrating the seal effectiveness of the Main Claystone into the Common Risk Segment (CRS) maps of the Geode Atlas (Kortekaas et. al., 2023) has already lead to significantly lower risk of present and working top seal in the southern Dutch offshore for potential CO₂ storage.

Recommendations for further study

Following a similar procedure, a future research could be focused on the southern NL onshore sealing potential of the Main Claystone, to expand the suggested GDE and sealing capacity maps. However, for further refinement and expansion of the GDE-Seal capacity maps, more core data from the RBSM has to be retrieved in the future. In this way, extensive lab measurements can provide more representative Poro./Perm. diagrams as well as detailed sedimentological analysis of the formation and direct sealing capacity measurements both through MITs and even direct CO₂ injection tests. Further investigation on the topic could include an extensive analysis on fault distribution/mapping and offsets/fault throws in the area, in order to identify potential risky faults able to compromise the top seal due to juxtaposition. Another more site specific research could be an investigation on any crestal faults present in known fields which could provide vertical migration (leak) paths through the RBSM for the stored CO₂. Finally, a future in depth pressure and overpressure analysis of the formation inside the same study area is highly recommended.

Conclusions

The Main Claystone Formation has a large sealing potential over most of the area of interest. Although continental in origin, the formation has been deeply buried resulting in increased level of compaction and stratification, diminished porosity and permeability with high levels of illite and anhydrite enrichments. The sealing capacity of the formation is primarily controlled by the composition and the stratification (strength). Particularly, is highly dependent on the clay content (especially on the illite content), the laminated or blocky-massive character and the anhydrite content. Structural elements such as erosional unconformities, however, can compromise the top seal effectiveness. The case of the P11-field and surrounding areas is a clear example of a region severely impacted by the early Cretaceous uplift and erosion associated with the Winterton High.

The regional sealing capacity map predicts that areas characterized predominantly by blocky/massive, anhydritic claystone facies can sustain column heights more than 465m, with a potential maximum value reaching more than two (to three) times larger values. Conversely, regions of dominant calcareous/dolomitic, laminated, silty claystone/shale facies can sustain a column height above 425m, with a maximum value measured at 465m. Finally, regions containing mostly sand-rich silty claystone facies, cannot withhold more than 145m of CO_2 and with or without the influence of erosion, are not expected to retain significant column heights, so they should be avoided for future exploration.

Overall, the results under the current study indicate a new very promising candidate efficiently acting as a top seal in the southern part of the Netherlands. The Main Claystone should continue being considered in future updates of the CRS maps in the Geode Atlas (https://www.geodeatlas.nl) as it is capable of minimizing the risk associated with the top seal effectiveness in the southern offshore.

Acknowledgements

I would like to express my sincere gratitude to all those who supported me throughout the completion of this report. My deepest appreciation goes to my supervisor(s) Dr. Aart-Peter van den Berg van Saparoea, Prof. Liviu Matenco and Fred Beekman for their invaluable guidance, encouragement and constructive feedback. I am also grateful to my colleagues and peers for their insightful discussions and collaboration.

Special thanks are due to Sofie van Driel and Dr. Daan den Hartog Jager for their exceptional support, motivation and assistance, which greatly enriched the quality of this work. Finally, I extend my thanks to my family and friends for their unwavering support and understanding during this journey.

References

- Aigner, T., & Bachmann, G. H. (1992). Sequence-stratigraphic framework of the German Triassic. *Sedimentary Geology*, 80(1-2), 115-135.
- DINOloket
- Geluk, M. C., & Röhling, H. G. (1997). High-resolution sequence stratigraphy of the Lower Triassic 'Buntsandstein'in the Netherlands and northwestern Germany. Geologie en Mijnbouw, 76, 227-246.
- Geluk, M. C. (2005). Stratigraphy and tectonics of Permo-Triassic basins in the Netherlands and surrounding areas. Utrecht University.
- Geluk, M. C., Wong, T. E., Batjes, D. A. J., & De Jager, J. (2007). Permian. *Geology of the Netherlands*, 63-83.
- Global CCS Institute
- Kombrink, H., Doornenbal, J. C., Duin, E. J. T., Den Dulk, M., Ten Veen, J. H., & Witmans, N. (2012). New insights into the geological structure of the Netherlands; results of a detailed mapping project. *Netherlands Journal of Geosciences*, *91*(4), 419-446.
- Kortekaas, M., R. Bouroullec, S. Peeters, M. van Unen, M. Swart, D. den Hartog Jager, E. Wiarda, M. Nolten, and K. Beintema. (2023). Play 7 Rotliegend. https://www.geodeatlas.nl/pages/play-7-rotliegend.
- McKie, T., & Kilhams, B. (2025). Triassic. *Geology of the Netherlands, second edition. Amsterdam University Press (Amsterdam)*, 155-183.
- NLOG
- Palermo, D., Aigner, T., Geluk, M., Poeppelreiter, M., & Pipping, K. (2008). Reservoir potential of a lacustrine mixed carbonate/siliciclastic gas reservoir: The Lower Triassic Rogenstein in the Netherlands. *Journal of Petroleum Geology*, 31(1), 61.
- Peryt, T. M. (1975). Significance of stromatolites for the environmental interpretation of the Buntsandstein (Lower Triassic) rocks. *Geologische Rundschau*, *64*, 143-158.
- Petrel subsurface software | SLB
- Purvis, K., & Okkerman, J. A. (1996). Inversion of reservoir quality by early diagenesis: an example from the Triassic Buntsandstein, offshore the Netherlands. In Geology of Gas and Oil under the Netherlands: Selection of papers presented at the 1983 Iternational Conference of the American Association of Petroleum Geologists, held in The Hague (pp. 179-189). Dordrecht: Springer Netherlands.
- Smith, D. A. (1966). Theoretical considerations of sealing and non-sealing faults. *AAPG Bulletin*, *50*(2), 363-374.
- Spatial without Compromise · QGIS Web Site
- Van Adrichem Boogaert, H.A. & Kouwe, W.F.P. 1994. Stratigraphic nomenclature of The Netherlands; revision and update by RGD and NOGEPA, Section E, Triassic. Mededelingen Rijks Geologische Dienst, 50, 1-28

Appendix

A) Summary of wells used:

OFFSHORE NL WELLS	P15-14	Q16-02	MDZ-01	53/12-02
P04-01	P15-17	Q16-04	MDZ-02	53/12-03
P05-02	P15-E-02	Q16-FA-101-S1	MRK-14	53/14-01
P06-06	P15-F-01	L07-17	MON-03	53/16-01
P06-01	P18-01	K18-06	MSB-01	53/18-01
P06-D-01	P18-02	K18-G-04	NWK-02	53/19a-01
P06-04A	P18-03	P01-01	SCH-01	54/01-01
P06-A-07	P18-A-02	P01-02	SPL-02	54/01a-03
P07-01	Q04-01	P01-03	SRM-01-VE	54/01b-02
P08-01	Q04-02	P01-04	SRM-02	54/01b-04
P08-06	Q04-06	P01-05	SRM-04	54/11-01
P09-01A	Q04-07	P01-06	STM-01	
P09-07	Q04-08	P01-07	VAL-01	
P09-09	Q04-B-01	P01-08	WAS-23-S2	
P10-01	Q05-01	P02-01	WIM-01	
P10-02	Q05-02	P02-02	WLK-01	
P10-03	Q05-03	P02-03	WOB-01	
P10-04	Q05-05	P02-04	ZSRM-01	
P11-01	Q07-01	P02-07	UK OFFSHORE	
F 11-01			WELLS	
P11-02	Q07-02	P02-08	50/16-01	
P11-03	Q07-04	P02-SE-02	50/21-01	
P11-04	Q07-05	P02-SE-02-S1	50/21-02	
P11-05	Q07-07	Q08-A-02	50/26-01	
P11-06	Q08-01	Q08-A-03	50/26a-02	
P11-07	Q08-02	ONSHORE NL	50/26a-03	
D11 00	009.07	WELLS	E0/262 04	-
P11-08	Q08-07	AMS-01	50/26a-04	
P11-09	Q08-B-01	STH-01	50/26a-07	-
P11-10	Q10-02	ALK-01	50/26b-05	
P11-A-01	Q10-03	ARV-01	50/26b-06	
P11-A-02A	Q10-04	BAC-01	50/26b-08	
P11-A-03	Q10-05	BKL-01	52/05-01	
P12-01	Q10-06	BKLM-01	53/04-02	
P12-03	Q10-A-02	BKLM-01-S1	53/04a-05	
P12-04	Q10-A-03	BUM-01	53/04a-09	
D12 44			F2/0F 04	
P12-11	Q10-A-04	EGMB-01	53/05-01	
P12-12	Q10-A-04 Q10-A-05	EGMB-01 EGZ-01	53/07-02	
P12-12 P12-A-01	Q10-A-04 Q10-A-05 Q11-01	EGMB-01 EGZ-01 EVD-01	53/07-02 53/08-01	
P12-12	Q10-A-04 Q10-A-05	EGMB-01 EGZ-01	53/07-02	

P14-01	Q13-03	HLO-01	53/10-02
P15-01	Q13-04-S1	KDZ-02	53/12-01

B) Column heights calculation:

• Air-brine capillary pressure (laboratory) data can be obtained from air-mercury data by the following conversion:

$$Pcg_b = Pca_Hg \bullet \sigma_2 \bullet \cos \theta_2 / \sigma_1 \bullet \cos \theta_1$$

Where:

Pcg-b = CO₂-brine capillary pressure (reservoir), psia

Pca-Hg = air-mercury capillary pressure, psia

 σ_2 = interfacial tension between CO₂ and brine (reservoir), dynes/cm (30) OR for air= (50)

 θ_2 = contact angle between CO₂ and brine (reservoir), degrees (30) OR for air=(0)

 σ_1 = interfacial tension between air and mercury, dynes/cm (480)

 θ_{1} = contact angle between air and mercury, degrees (140)

• The maximum height H of the CO₂ column that can be sealed by each sealing lithology can be calculated by using the equation of Smith (1966):

$$H= P_{b(seal)}/1.42*(\rho_b-\rho_g)$$

Where:

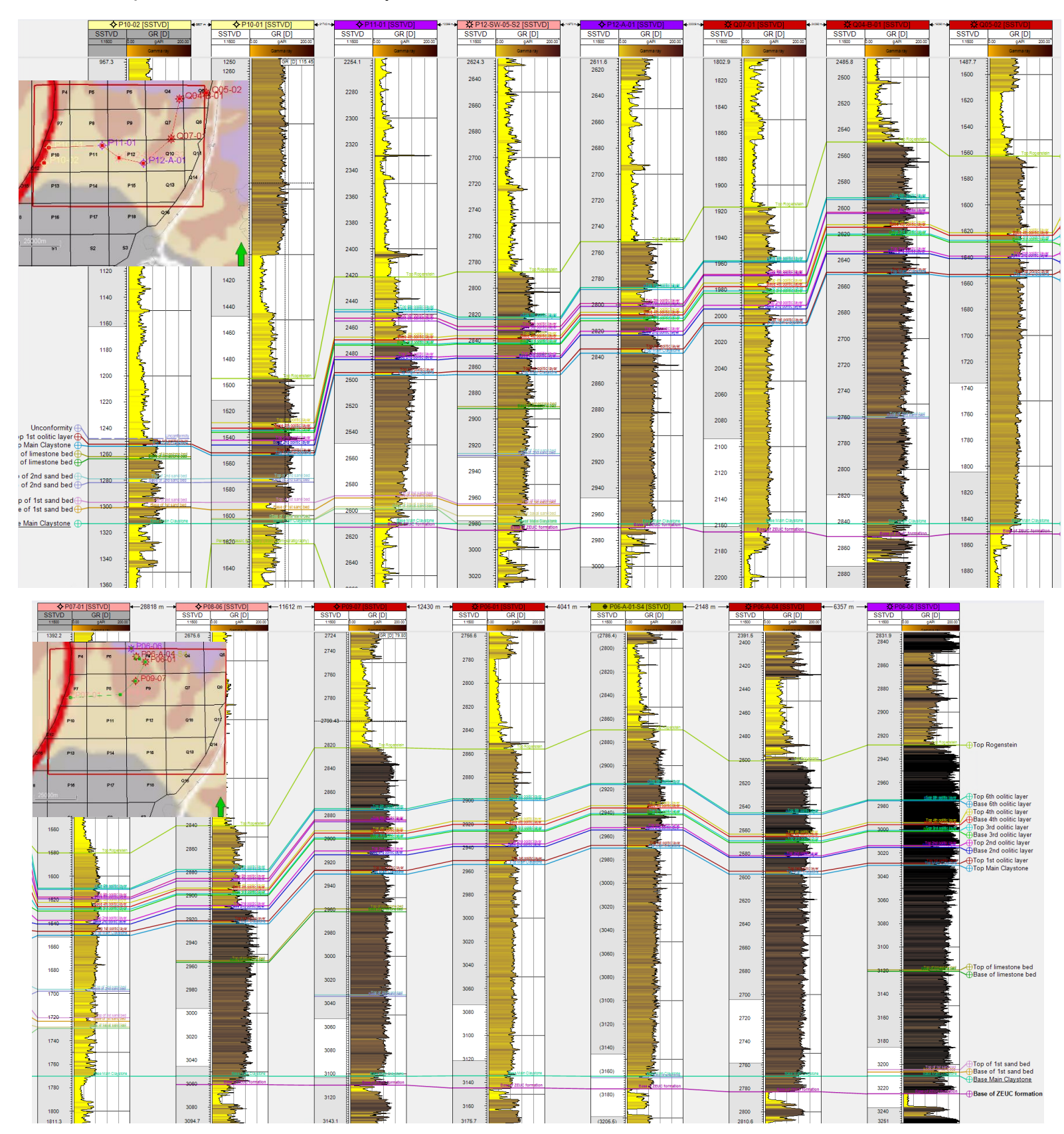
P_{b(seal)}= capillary breakthrough pressure of the seal (in psia) at reservoir conditions

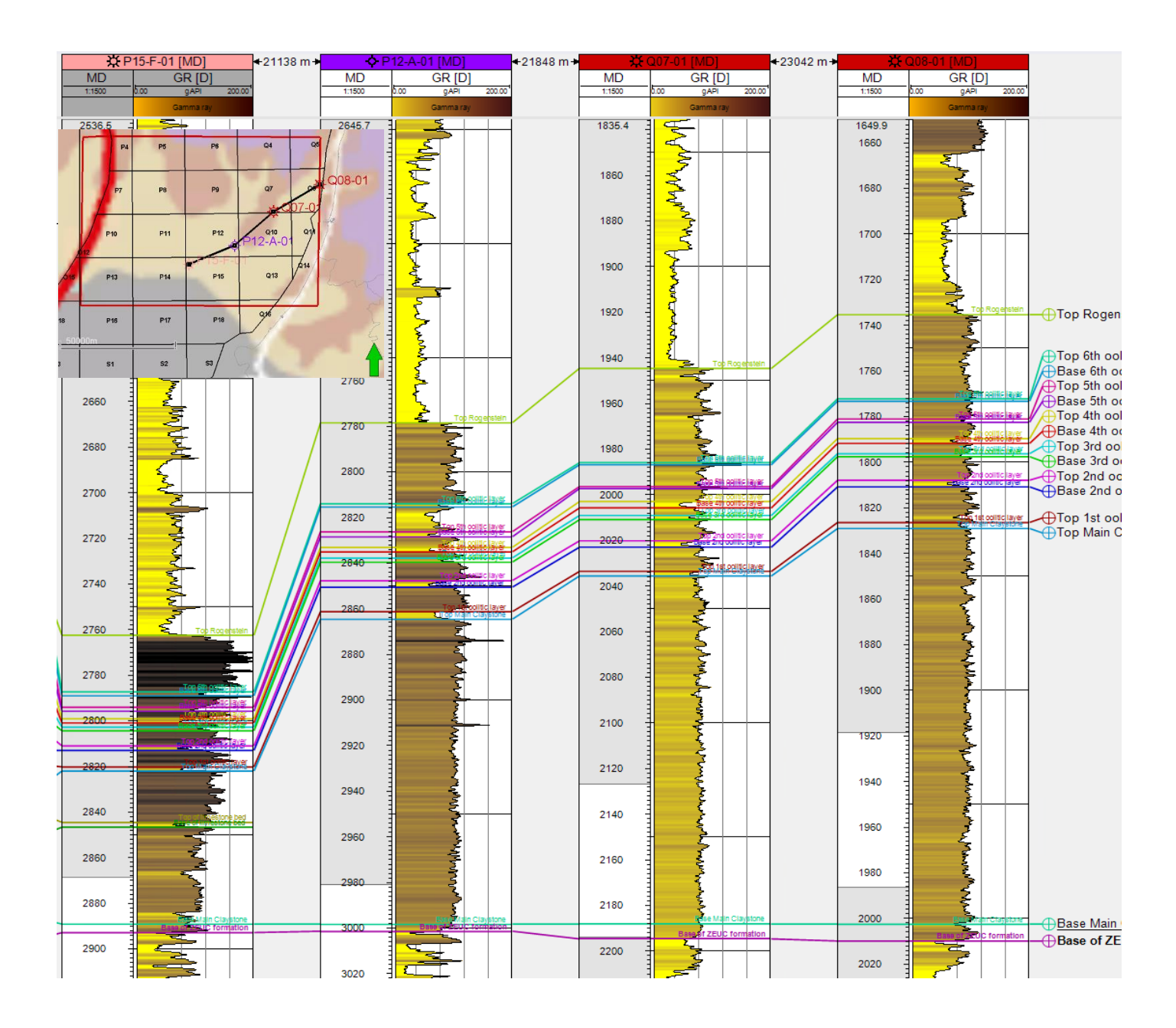
 ρ_b = subsurface density of the brine (in g/ml)

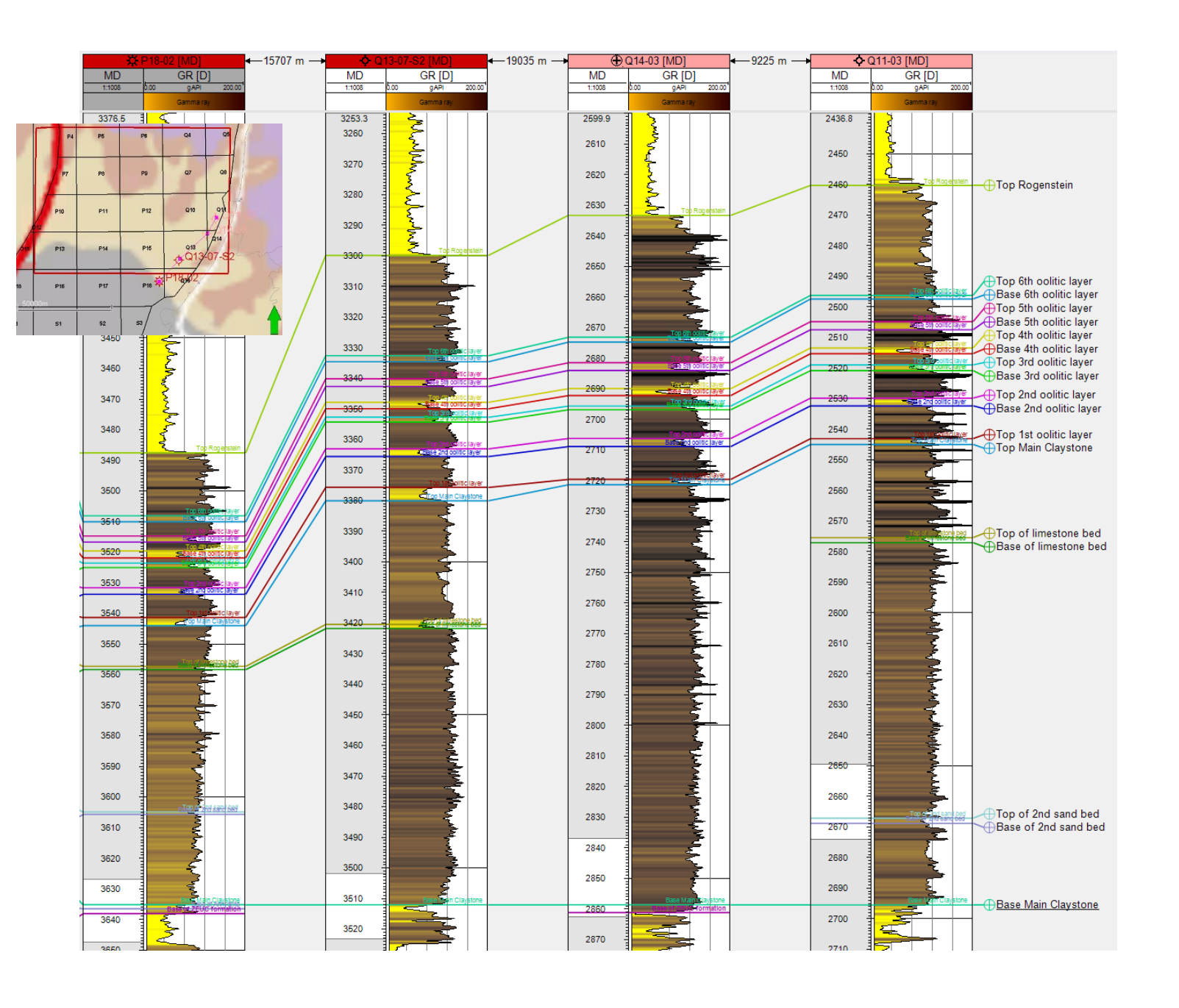
 ρ_g = subsurface density of the CO₂ (in g/ml)

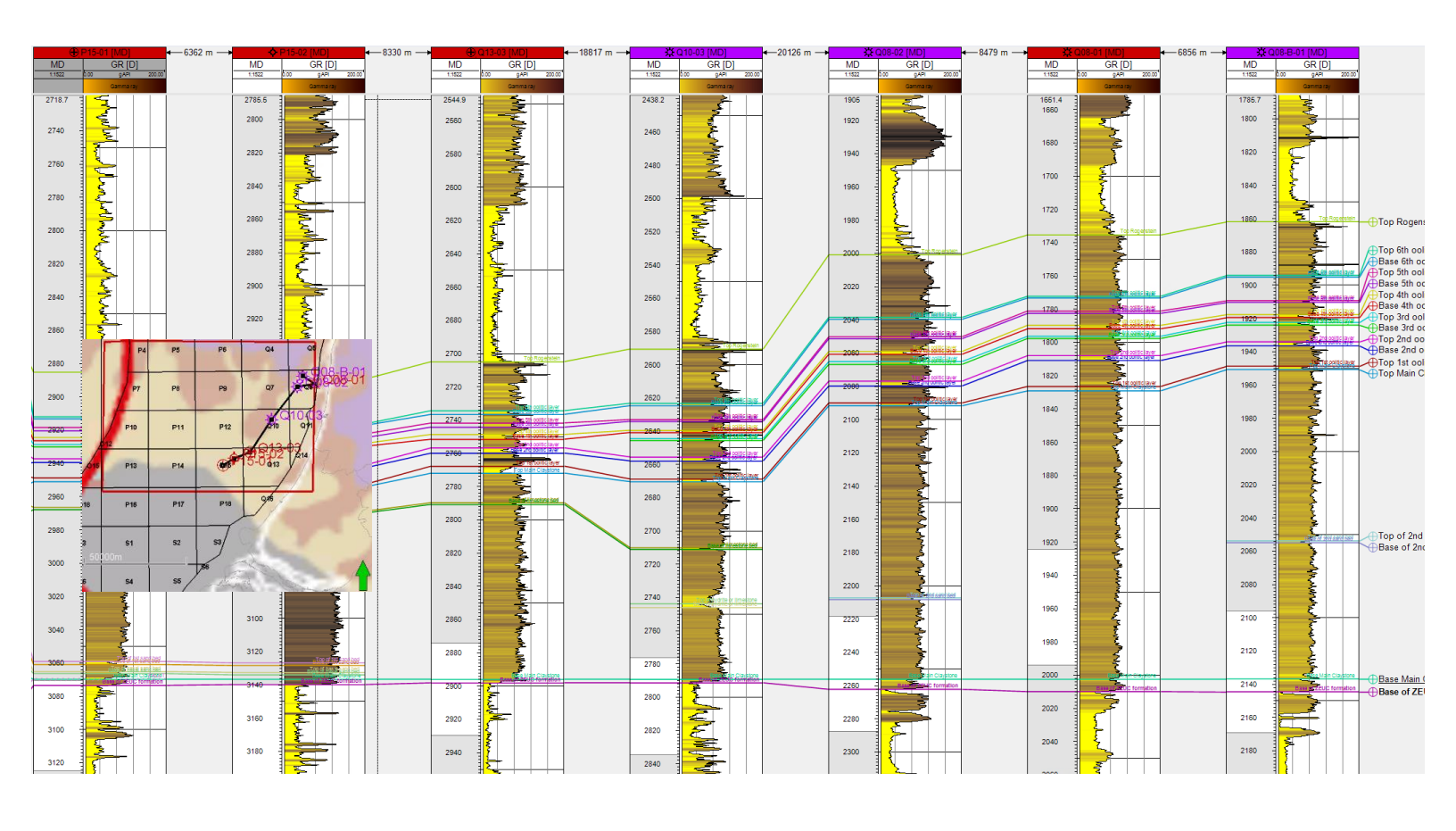
1.42 is a unit's conversion factor.

C) Additional well correlation panels:

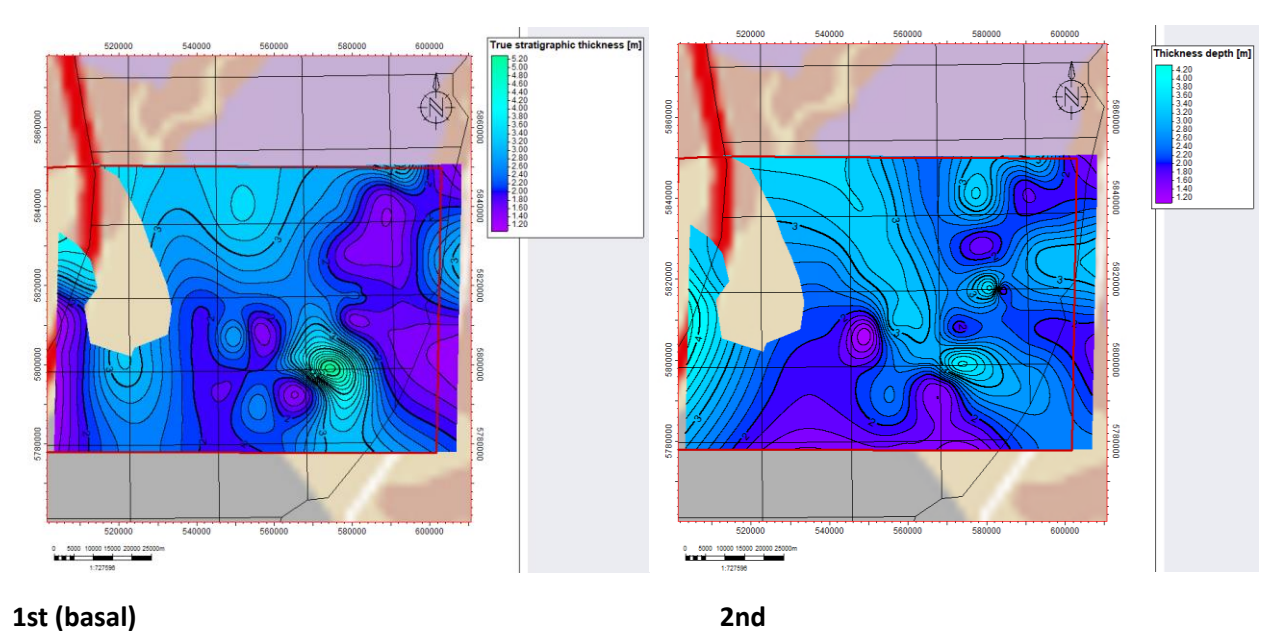


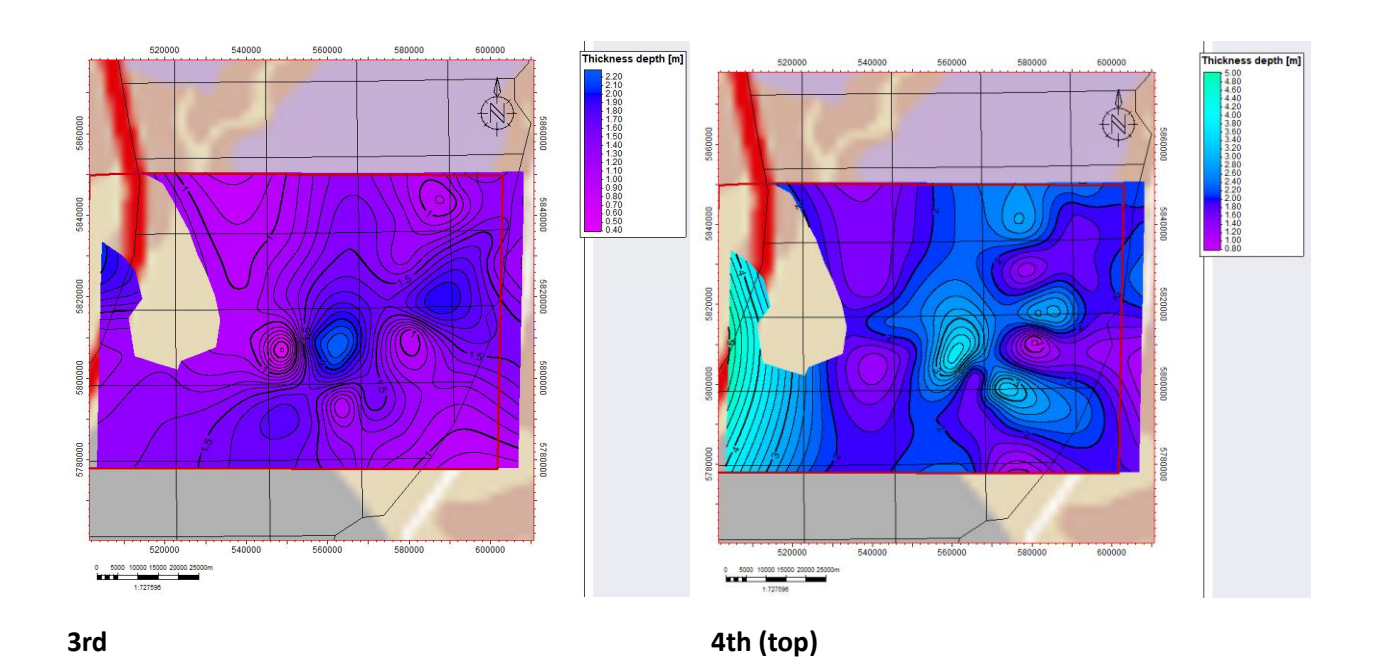






D) Thickness maps of the Rogenstein oolites:





E) Core photos:





Well AMS-01: Personal photo of the core, depositional environment and Poro/Perm plots presented internally by the Geothermal team.

F) Nederweert formation (RBSN) distribution (through the Dinoloket database):

Geographical distribution



G) Depth vs overpressure plots for RBSM (internal database):

